Czech Technical University in Prague
Faculty of Electrical Engineering
Department of Control Engineering

Master's Thesis

Rijke Tube Organ

Author: **Krištof Pučejdl**
Supervisor: **Jiří Zemánek**
Academic Year: **2018/2019**

MASTER'S THESIS ASSIGNMENT

I. Personal and study details

Student's name: **Pučejdl Krištof** Personal ID number: **406514**

Faculty / Institute: **Faculty of Electrical Engineering**

Department / Institute: **Department of Control Engineering**

Study program: **Cybernetics and Robotics**

Branch of study: **Cybernetics and Robotics**

II. Master's thesis details

Master's thesis title in English:

Rijke Tube Organ

Master's thesis title in Czech:

Rijkeho trubice jako hudební nástroj

Guidelines:

The aim of this project is to turn a popular physical experiment called Rijke Tube into a musical instrument. The instrument should allow both a live performance with a musician and a recorded show with a MIDI sequencer.
1. Find a suitable design of the tube, heater, sensors, and actuators.
2. Create a mathematical model for control purposes.
3. Design feedback and feedforward filters to change characteristics of the tone - attack, decay, frequency, etc.
4. Create a demonstration of the instrument.

Bibliography / sources:

[1] Heckl, Maria A. "Active Control of the Noise from a Rijke Tube." Journal of Sound and Vibration 124, no. 1 (July 8, 1988): 117–33.
[2] Epperlein, J. P., B. Bamieh, and K. J. Astrom. "Thermoacoustics and the Rijke Tube: Experiments, Identification, and Modeling." IEEE Control Systems Magazine 35, no. 2 (April 2015): 57–77.
[3] Černý, L. 'Rijke's Tube - An Experimental Platform for Modeling and Control in Thermoacoustics.' Bachelor Thesis. Czech Technical University in Prague. (2017).
[4] Epperlein, J. P. 'Topics in modeling and control of spatially distributed systems.' Dissertation. University of California, Santa Barbara. (2014).

Name and workplace of master's thesis supervisor:

Ing. Jiří Zemánek, Ph.D., Department of Control Engineering, FEE

Name and workplace of second master's thesis supervisor or consultant:

Date of master's thesis assignment: **15.02.2019** Deadline for master's thesis submission: **24.05.2019**

Assignment valid until:
by the end of summer semester 2019/2020

Ing. Jiří Zemánek, Ph.D.	prof. Ing. Michael Šebek, DrSc.	prof. Ing. Pavel Ripka, CSc.
Supervisor's signature	Head of department's signature	Dean's signature

Abstract

Rijke tube is an old physical experiment demonstrating a spontaneous generation of sound in an open tube with a heat source. This phenomenon is well researched due to its parallel to other thermoacoustic systems. In this thesis, I revisit the experiment, focusing on its potential use of the Rijke tube as a musical instrument.

Presented novel approach lies within aplying modern control methods on the Rijke tube, and augmenting the previously investigated methods of suppression of the sound with new concepts of control objectives, including the amplitude regulation and active sound excitation.

First, I develop the time-domain mathematical model which considers the nonlinear aspects of the Rijke tube and as such extends the existing modeling approaches which are mainly focusing on frequency-domain system analysis.

Upon this mathematical model I design and test the control system, which utilizes a heater control and active acoustic control as two input methods. In combination, these two allow for enhanced acoustic performance of the Rijke tube, and provide a good foundation for further attempts on playing original musical pieces.

Last, but most importantly, I design and build the actual Rijke organ instrument using modern methods of fabrication and rapid prototyping, including 3D printing and laser-cutting. The organ allows the full demonstration of the control system and provides a platform for further research and development concerning the control of thermoacoustic instability.

Keywords: Rijke tube, Rijke organ, acoustic oscillations, thermoacoustic instabilities.

Abstrakt

Rijkeova trubice je starý fyzikální experiment, který demonstruje spontánní vznik zvuku v otevřené trubce se zdrojem tepla. Tento jev je zkoumaný zejména ve spojitosti s jinými termoakustickými systémy. V této práci jsem se k tomuto experimentu vrátil se zaměřením na jeho potenciální využití Rijkeovy trubky jako hudebního nástroje.

Prezentovaný originální přístup spočívá v aplikaci moderních metod řízení na Rijkeho trubici a rozšíření již dříve zkoumaných metod tlumení zvuku o nové koncepty, včetně regulace amplitudy a aktivního zvukového buzení.

Nejprve jsem vyvinul matematický model v časové oblasti, který uvažuje nelineární aspekty dynamiky Rijkeovy trubice a jako takový rozšiřuje existující modelovací přístupy, které se zabývají především analýzou systémů ve frekvenční oblasti.

Na základě tohoto matematického modelu jsem navrhnul a otestoval řídicí systém, který využívá regulaci tepelného zdroje a aktivní akustické řízení jako dvou vstupů do systému. Tyto metody společně umožňují lepší akustický projev Rijkeho trubky a poskytují dobrý základ pro další pokusy o hraní originálních hudebních skladeb.

Poslední, ale co je nejdůležitější, navrhuji a stavím vlastní Rijkeho varhany s využitím moderních metod výroby a rychlého prototypování, včetně 3D tisku a laserového řezání. Varhany umožňují plnou demonstraci řídicího systému a poskytují platformu pro další výzkum a vývoj týkající se řízení termoakustické nestability.

Klíčová slova: Rijkeho píšťala, Rijkeho varhany, akustické vibrace, termoakustická nestabilita.

Declaration

I hereby declare that I wrote the presented thesis on my own and that I cited all the used information sources in compliance with the Methodical instructions about the ethical principles for writing an academic thesis.

Prague, May 24, 2019

Author's signature

Acknowledgement

I would like to thank my supervisor Jiří Zemánekfor initiating the idea beneath this thesis, and for his insightful hints which helped me to navigate throughout the difficulties associated with the topics in my work. I would also like to thank my friend Martin Horejš for offering me his helpful hand during the laborious parts of the manual construction involved, and my friend Jan Filip for his help regarding the written part of the work. Last, and most importantly, I can not possibly express my full gratitude to my family for their limitless and unprecedented love and support.

Contents

Acronyms

CAD	Computer Aided Design.
CTCR	Cluster Treatment for Characteristic Roots.
DAQ	Data Acquisition.
FDM	Finite Difference Method.
FEM	Finite Element Method.
FFT	Fast Fourier Transform.
FIR	Finite Impulse Response.
LFT	Linear Fractional Transformation.
LPV	Linear Parameter-Varying.
LTI	Linear Time-Invariant.
LTI-NMTDS	Linear Time-Invariant Multiple Time-Delayed System of Neutral type.
LTV	Linear Time-Varying.
PBH	Popov-Belevitch-Hautus.
PID	Proportional, Integral and Derivative.
PWM	Pulse-Width Modulation.
QPmR	Quasi-Polynomial mapping based Root finder.
RMS	Root Mean Square.
TDI	Time-Delayed Integral.

1 Introduction

Discovered in 1859 by a Dutch physicist Petrus Leonardus Rijke, the Rijke tube is an acoustically attractive experiment, often used as a demonstration during scientific-popular lectures. In this thesis, I use the Rijke tube as the base principle for a musical instrument - a Rijke organ.

1.1 Motivation

The unexpected origin of sound in the Rijke tube, which lacks any immediately apparent reason, brings peoples attention, yet, there have been only a few attempts of some more advanced ways of exhibiting this effect. Considering the Rijke tube as the base for a musical instrument in combination with modern methods of automatic control is a novel idea and offers many engineering challenges.

1.2 Related work

Most of the academic work concerning Rijke tube relates to the investigation of thermoacoustic systems in general and aims at the practical application in different industry devices, such as furnaces, engines and other types of combustion systems. The thermoacoustic instability featured in these systems is generally undesirable, causing either loss of efficiency or even harmful conditions. Rijke tube provides a good laboratory experiment providing close enough representation of these phenomena so that researchers can develop methods of combating the instabilities.

Little to no scientific work has been done concerning the intentional excitation and control of the instabilities in the tube towards a musical performance. There are several existing attempts on building a Rijke tube-based organ, but the documentation is minimal, and the concepts only contain the very basic form of the Rijke tube experiment. Professor Bryan H. Suits at the Michigan Technological University constructed an organ consisting of five electrically actuated Rijke tubes[1] and successfully demonstrated its manual operation. On his website, he provides a basic description of the construction. A very similar concept can be found at a German-based YouTube channel[2], featuring a nice mechanical execution but with no documentation.[3] Last, a musician Alastair Galbraith from New Zealand created a large 'flame organ', which consisted of many flame-operated Rijke tubes connected to a piano-like keyboard. Despite being the largest attempt, it provides the least reference for my work, due to its difference in actuation and overall philosophy of scale and design.

[1] pages.mtu.edu/~suits/electronics/ElecRijke.html
[2] www.youtube.com/user/xofunkox/featured
[3] www.youtube.com/watch?v=qdII8sMYinY

1.3 Contributions

Besides contributing to the exploration of unorthodox musical instruments and creating an interesting demonstration of a complex physical phenomenon, this work also expands on possibilities of active automatic control of the Rijke tube-like system and also its mathematical modeling, in particular concerning the time-domain simulation. Existing investigations in the domain are predominantly oriented in the frequency-domain analysis of the thermoacoustic systems, and my aim is to transition into time-domain is motivated by the possibility of model-based control design.

1.4 Outline

This thesis summarizes my four-month effort on this project and approximately follows the actual timeline of the work. In Chapter 2 I give a brief introduction of the physical background of the Rijke tube dynamics which I then implement into a mathematical model in Chapter 3. Next, in Chapter 4 I describe the prototype Rijke tube platform on which I conducted the experiments, and tested the control systems developed in Chapter 5. The prototype platform also served as a test bed for finding the limitations of the setup and determining the design and engineering choices that I made towards the final organ build described in Chapter 6.

2 | Physics of the Rijke Tube

In this section, I describe the physical phenomena which significantly contribute to forming the overall dynamics of the Rijke tube, mainly to set the stage the following Chapter 3 where I construct a mathematical model. This chapter is only a brief review of the physics behind the system, and does not aim to give a complete in-depth description or to advance the current understanding.

In its complete form, a Rijke tube is a complex physical system that involves interaction between thermal and acoustic domains. There are wave as well as fluid flow dynamics involved in the behavior of the velocity of the gas in the tube, accompanied by numerous means of energy dissipation. Many of these aspects are inherently nonlinear and while the overall performance, which was first hypothesized by Lord Rayleigh [1], is well understood and documented by researchers, giving an exhaustive explanation of all the phenomena in terms of equations and rigorous physical laws still presents a great challenge.

The fundamental underlying principle that gives birth to the acoustic instability is an initial airflow velocity and pressure gradient generated in the tube by the thermal energy input from the heater. Under the right conditions, including the heat input power, spatial proportions of the tube and pressure wave reflections at the ends of the tube, a cyclic change of the sound pressure emerges in the tube, which affects the heat transfer and leads to amplification of the sound pressure waves up to some limit cycle saturation. Epperlein provides a nice diagram explaining the conceptual working of the amplification (See Figure 1.2 in [2], or Figure 3 in [3]), which helps to get a basic understanding of the underlying principle.

Three main components, which are inextricably intertwined, are the sound forming acoustic instability, unstable heat release, and buoyancy[1] induced mean airflow. These effects coexist in a relationship where the acoustic instability in the form of self-amplifying standing wave in the tube can only exist in the presence of the airflow and unsteady heat release, while the latter is induced by the acoustic instability itself and further influenced by the mean airflow. Despite the strong coupling, the key features of the phenomena can be described separately.

2.1 Acoustic of the Resonant Pipe

The fundamental acoustic mode of a resonant pipe of length l forms a standing half-wave in the pipe. Hence the theoretical wavelength λ of the first harmonic frequency equals twice the length of the pipe. In reality, however, it is observed that the wavelength is slightly larger, as $\lambda > 2l$, as the actual common node or antinode of the acoustic waves slightly extends past the ends of the tube. This extension is referred to as *end correction* and it is believed to be proportional to the hydraulic

[1] Not to be confused with Beyoncé.

radius r (inside radius) of the tube, albeit there is no proven and universally accepted value of the proportionality constant. Lord Rayleigh [1, 4] was the first experimenter to publish a figure for the closed pipe end correction $0.6r$. In literature, used values are commonly ranging from $0.6r$ to $1.2r$.

The standing acoustic wave is formed due to reflections at the tube's extended virtual ends. There are two key aspects to the reflection, one of which being the change of the direction of the wave travel, which corresponds to the change of sign of the wave function. The other aspect is the attenuation of the wave, which in general depends on the diameter of the tube and the frequency of the acoustic wave. Levine and Schwinger presented in [5] a thorough examination of the behavior of the reflection coefficient given by

$$R_\mathrm{r} = -|R_\mathrm{r}|e^{2ikl_\mathrm{e}} \tag{2.1}$$

where l_e is the value of the end correction and and $k = 2\pi/\lambda = \pi/l$ is the wave number, and offered the approximate formula for its magnitude

$$|R_\mathrm{r}| \approx -\exp\left[-\frac{(ka)^2}{2}\right]\left[1+\frac{(ka)^4}{6}\left(\log\frac{1}{\gamma\, ka}+\frac{19}{12}\right)\right], \quad ka \leq 1\,, \tag{2.2}$$

where γ is the adiabatic ratio, and ka is nondimensional quantity commonly referred to as Helmholtz number, and it is a product of wave number and tube diameter. In Figure 2.1a I show the plot of $|R_\mathrm{r}|$ for ka ranging from 0 to 1. By fixing the tube diameter and expressing ka as

$$ka = \frac{\pi r}{2l} = \frac{\pi r f_0}{\bar{c}}\,, \tag{2.3}$$

I can evaluate $|R_\mathrm{r}|$ as a function of f_0 and show the resulting attenuation of the fundamental frequency in Figure 2.1b.

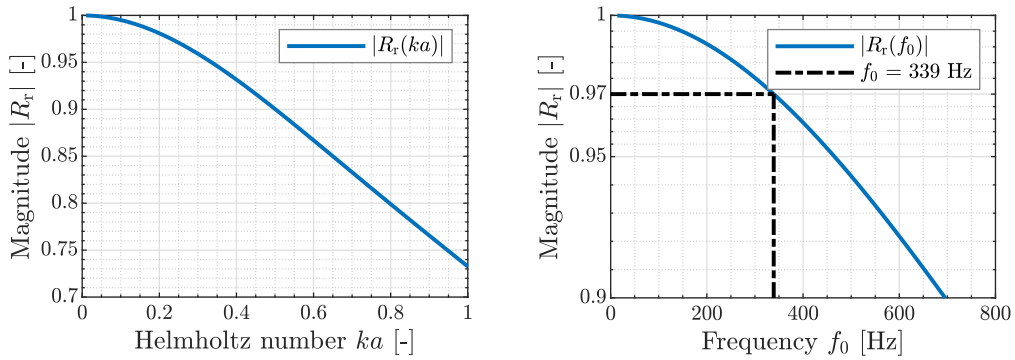

Figure 2.1: Magnitude $|R_\mathrm{r}|$ of the reflection coefficient as a function of Helmholtz number ka (a) and as a function of frequency f_0 for $r = 4.071$ cm (b).

Clearly, the attenuation grows with the frequency, which is the essential element to this physical phenomenon. It effectively prevents higher harmonic frequencies to become dominant in the dynamic response of the system, unless the fundamental mode is artificially suppressed, as observed by many researchers and recently explained by Zallugholu and Olgac in [6]. I describe the specifics of modeling of the reflections in Section 3.5.

2.2 Unsteady Heat Release

The dynamics of the heat transfer from the heat source to the gas in the tube is a key aspect of the Rijke tube behavior. The heat transfer coefficient, which essentially describes how much energy is being transferred from the heat source to the gas in the tube, generally is proportional to the temperature of the heat source, and also depends on the velocity of the gas flow. Both of these quantities are variable in time; in fact, they are mutually dependent. As their values fluctuate in time, the heat transfer coefficient also exhibits its own dynamical behavior, instead of just instantaneous dependency given by the static laws. The dynamics vary for different types of heat sources and further complicates for flame or other combustion-based inputs. For the heating wire based source, which I consider in this work, the description is more tangible. Inspired by observations on Rijke tube, Lighthill analyzed these dynamics thoroughly in [7], and simplified description of his findings can be found in [2]. Essentially, the heat output from the heater has to traverse through some boundary layer of stagnant gas in the proximity of the heater. This boundary layer is established due to skin friction on the surface of the heater wire. This propagation of the heat introduces a first-order lag in the dynamics binding the velocity and heat transfer fluctuations.

Lighthill shows in [7] that this lag, albeit small, is indeed an important aspect of the whole functioning of the Rijke tube, and thus quintessential for the validity of the mathematical description. I go over the actual governing equations in more detail in the description of mathematical modeling in Section 3.3.

2.3 Dynamics of the Convective Flow

Last considerable contributor to the overall Rijke tube dynamics is the buoyancy-induced convective airflow. This phenomenon is also called stack effect or chimney effect and does not need much introduction, as it is observed commonly in all kinds of structures that implement some internal heating and allow vertical airflow. In a straight vertical tube with smooth internal walls, such airflow can be well approximated by laminar airflow. That is, however, with ignoring the damping effects on the boundaries at the tube ends and along its walls, and possible defects to the laminar flow caused by the bodies of the heater and microphone in the tube. Moreover, there are random perturbations caused by the motion of the air around the ends of the tube.

I found during the experiments that especially the latter has a strong detrimental effect on the acoustic performance of the tube. For a smaller size of the Rijke tube in particular, it takes very little to disturb the upward flow and cause the acoustic instability to either vary in amplitude or even die out temporarily. A full explanation of the flow dynamics is well beyond the scope of this work and instead of vague attempts, I present the much-simplified approach to mathematical modeling of the buoyancy flow in Section 3.4 along with the arguments supporting the plausibility of the approximations w.r.t. the completed model.

3 | Mathematical model

There are several approaches to modeling of the simplified Rijke tube system. Given its numerous nonlinear aspects, it depends on the purpose of the mathematical model whether a linearization or straightforward neglection is acceptable. In this chapter, I first present and discuss various approaches concerning the related developments as well as this work, offer some justification to the consequent choices I made and finally derive a model which I later use for experiments and control design.

3.1 Related work

Most development in this topic carried out in the past was concerned with the modal behavior of the Rijke tube-like system, including stability analysis respective and plant and controller design. The methods used were almost exclusively limited to frequency-domain. Motivated by either suppression [8, 9, 3, 10], or excitation [11] of the acoustic resonances in the system, different techniques were used to obtain approximate transfer functions of the system linearized in certain operation point, and these were then inspected using various methods of frequency and modal analysis. Despite the apparent nonlinearities in the system, its frequency and mode shape is well described by linear theory [12, 13] and therefore in most related work the development is based upon linearized models.

My aim within this work is to develop a mathematical model which would be feasible for time-domain simulations. Ignoring the nonlinearities and the dynamics of secondary phenomena, including the buoyancy-aided convection flow in the tube, and its influence onto the primary thermoacoustic behavior is no longer warranted if one wants to model the true behavior of the system without specifying the operating conditions.

A resounding succes in modeling the nonlinear self-excited oscillations was presented by Dowling in [12], where the results of numerical simulations clearly feature the limit cycle behavior (See Figure 3 in [12]). Dowling derived a model based on a set of partial differential wave equations representing the traveling pressure and velocity waves in both directions along the tube length combined with boundary condition on the tube ends and nonlinear velocity-dependent heat release rate. However, the nonlinear effects were implemented mostly empirically, using saturations on the otherwise linear velocity dependent heat release rate. Dowling also included simplified physics of the flame, and the overall geometry of the setup was slightly different. The core principle of modeling using reflections of traveling waves was also used by Zalluhoglu and Olgac in [9, 6], where the idea of using time delays to interconnect the wave equations expressed in selected positions along the tube is presented, which yields results that are in good agreement with the physical reality in the frequency-domain.

Another approach to time-domain simulations is high fidelity Finite Element

Method (FEM) or Finite Difference Method (FDM) modeling, some of which is successfully applied to the thermoacoustic instabilities in Rijke tube in [14]. Despite its possible advantages in terms of completeness of the description and superior ability to capture the spatial distribution of the variables, related software requirements and consequent limitations, as well as extensive computation cost, rendered this approach inferior for this work.

Instead, I decided to adopt the core modeling idea from Dowling and even more so from the recent application presented by Zalluhoglu and Olgac, albeit the latter limits to linearized case and frequency-domain analysis, and, therefore, only serves as a reference in the initial part of the model derivation. For easier referencing and clarity I follow the notation used in [9, 6] in the subsequent derivations.

The possible risk associated with using the given framework for time-domain simulations is the lack of robustness and sensitivity to numerical errors. There is quite a substantial theory developed for time-delay system in terms of stability analysis and control system design based on frequency-domain methods [15, 16]. However, time-domain numerical simulations of a model which employs multiple time delays as a source of rich oscillatory dynamics are unorthodox, and there appears to be no substantial development to serve as a reference.

3.2 Conceptual model description

As stated before, this domain involves dealing with the mechanics and thermodynamics of a continuum in the form of the fluid (air) inside and also around the tube and the tube itself. For any reasonable attempt at a simplified mathematical description, one needs some anchoring points in terms or initial assumptions.

1. There is a stable natural buoyancy-aided mean airflow in the tube caused by the heat power input.
2. Mean airflow has low velocity and negligibly small Mach number.
3. The acoustic wave propagation, as well as the mean flow, are one-dimensional events w.r.t. the length of the tube.
4. The average mean flow quantities such as the speed of sound $\bar{c}$ and density $\bar{\rho}$ are constant across the volume of the tube.
5. The heating zone is narrow in the direction of the tube axis, compared to the length of the tube.
6. There are no means of energy dissipation other than the losses at the acoustic wave reflections.

Assumptions 1-5 are commonly adopted in related literature. The last condition seems to be often present without being directly specified, especially in literature which considers linear models and focuses on the inspection of the modal behavior. Heckl [8] mentions energy dissipation and consequent attenuation of the sound waves caused by sound radiation along the tube wall (Stokes boundary layer) which is otherwise seldom considered to be a nonnegligible phenomenon. Next, there are multiple causes of heat energy dissipation accompanying the complex energy transfer from the heater to the acoustic instability. Later in this section, I account for some of these phenomena by using a nonlinear model for the efficiency of the velocity

dependent heat transfer. The validity of the very first assumption is also further discussed in Section 3.4 where I argue that keeping such assumption for the purposes of the simulation model would compromise its usability.

The entry point to the presented modeling approach is the well-known general form of d'Alembert solution of the linear wave equation for acoustic pressure and velocity fluctuations $\tilde{p}$ and $\tilde{u}$.

$$\tilde{p}(x,t) = f\left(t - x/\bar{c}\right) + g\left(t + x/\bar{c}\right) \tag{3.1}$$

$$\tilde{u}(x,t) = \frac{f\left(t - x/\bar{c}\right) - g\left(t + x/\bar{c}\right)}{\bar{\rho}\bar{c}} \tag{3.2}$$

Hence, at each point, the function of the acoustic pressure is a combination of two waves traveling in opposing directions. Neglecting the energy gain or dissipation along the path which the wave has to traverse—in this case the length of the tube—it holds that such traveling waves evaluated in different positions are causally related through time delays. On the open tube ends, the wave reflects and travels back with the amplitude and phase given by some reflection coefficient. By evaluating the functions $f(t)$ and $g(t)$ at the important cross-sections along the length of the tube and defining respective time delays between the cross sections, the spatially distributed problem can be substituted with a time-delay system. Following the assumptions, the important cross sections, in this case, are the heater zone, the microphone zone, and both ends of the tube. Schematic drawing of the Rijke tube with denoted cross sections is in Figure 3.1a and the corresponding block diagram for such system is given in Figure 3.1b. Note that in the presented setup, the microphone is placed in the downstream section of the tube. Later in this work, I experiment with the alternative placement and discuss the difference between the two. The downstream placement offers some advantages for the model analysis, and it appears to be used exclusively in the related work and experiments, and it was used during the early physical experiments in this work.

Respective time delays τ_i correspond to the travel times for the acoustic wave between significant cross sections, hence $\tau_1 = x_\mathrm{u}/\bar{c}$, $\tau_2 = x_\mathrm{m,d}/\bar{c}$ and $\tau_3 = \left(x_\mathrm{d} - x_\mathrm{m,d}\right)/\bar{c}$. Functions interacting with the heating zone are governed by the heating zone transfer function $\mathbf{H}(s)$.

$$\begin{bmatrix} G_2(s) \\ F_3(s) \end{bmatrix} = \mathbf{H} \begin{bmatrix} F_2(s) \\ G_3(s) \end{bmatrix} \tag{3.3}$$

The specific modeling of the heat release is discussed in Section 3.3, for now, it suffices to assume $\mathbf{H}(s)$ to be a general transfer function. Next comes describing of the causal connection between the acoustic pressure variables via time delays indicated in Figure 3.1b.

$$\begin{bmatrix} F_2(s) \\ G_3(s) \end{bmatrix} = \mathbf{T} \begin{bmatrix} F_1(s) \\ G_5(s) \end{bmatrix}, \quad \mathbf{T} = \begin{bmatrix} e^{-\tau_1 s} & 0 \\ 0 & e^{-(\tau_2+\tau_3)s} \end{bmatrix}. \tag{3.4}$$

For the variables at the tube ends there are reflections taking place, and thus the opposing waves can be tied together via the respective reflection coefficients $R(s)$. In [9]

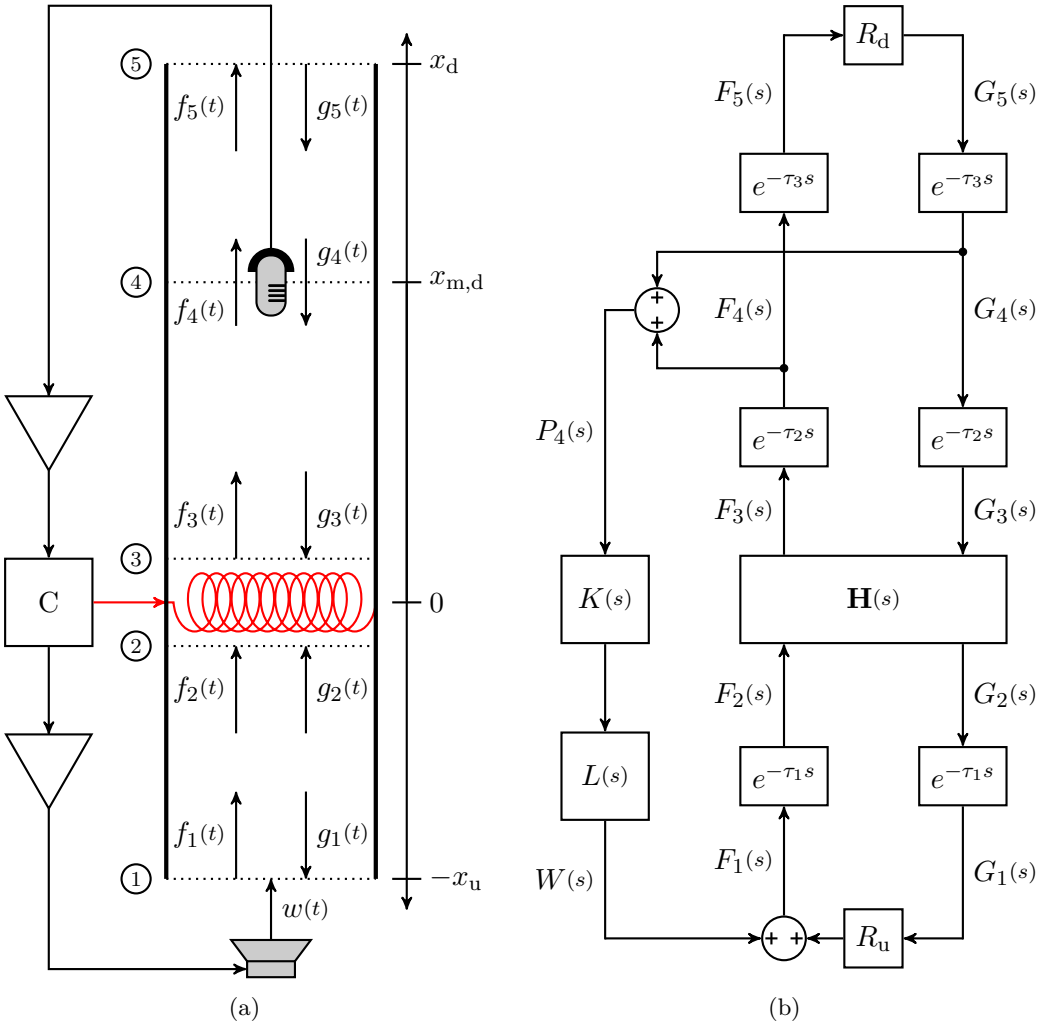

Figure 3.1: Schematic (a) and block diagram (b) representation of the simplified time-delay based model of the Rijke tube with downstream microphone placement.

these coefficients are modeled as a simple constant gain, but based on the physical principle described briefly in Section 2.1 I am convinced that such representation is not sufficient, and I discuss an alternative in Section 3.5.

At the upstream end of the tube, there is also the control signal $W(s)$ added to the reflected wave $F_1(s)$ as a Laplace domain representation of the acoustic pressure control input $w(t)$ induced by the loudspeaker.

$$\begin{bmatrix} F_1(s) \\ G_5(s) \end{bmatrix} = \mathbf{R} \begin{bmatrix} G_1(s) \\ F_5(s) \end{bmatrix} + \begin{bmatrix} W(s) \\ 0 \end{bmatrix}, \quad \mathbf{R} = \begin{bmatrix} R_\mathrm{u} & 0 \\ 0 & R_\mathrm{d} \end{bmatrix}. \tag{3.5}$$

Functions that enter the reflection can again be determined as time-delayed outputs from $\mathbf{H}(s)$, hence

$$\begin{bmatrix} G_1(s) \\ F_5(s) \end{bmatrix} = \mathbf{T} \begin{bmatrix} G_2(s) \\ F_3(s) \end{bmatrix}. \tag{3.6}$$

The feedback controlled signal $W(s)$ can now be expressed as

$$W(s) = K(s)L(s)\left(F_4(s) + G_4(s)\right) , \tag{3.7}$$

where $K(s)$ represents the user determined controller transfer function and $L(s)$ is a compound transfer function of all the feedback loop elements with nonnegligible dynamics. For the sake of simplicity and inspecting just the phenomena associated with thermoacoustic instabilities, it is beneficial to assume idealized components with $L(s) = 1$. For more precise control design which is to be implemented on the real platform, it is necessary to at least approximate the transfer function via some method of input-output system identification [10].

Once again using causal relationship, Eq. (3.7) can be rewritten as

$$W(s) = K(s)L(s)\left[e^{-\tau_2 s}\left(1 + e^{-2\tau_3 s}R_\mathrm{d}\right)\right]F_3(s) , \tag{3.8}$$

and further expressed in terms of the matrix equation for a couple of acoustic pressure variables $G_2(s)$ and $F_3(s)$ as

$$\begin{bmatrix} W(s) \\ 0 \end{bmatrix} = \mathbf{\Pi}\begin{bmatrix} G_2(s) \\ F_3(s) \end{bmatrix}, \quad \mathbf{\Pi} = \begin{bmatrix} 0 & 0 \\ 0 & K(s)L(s)e^{-\tau_2 s}\left(1 + e^{-2\tau_3 s}R_\mathrm{d}\right) \end{bmatrix} . \tag{3.9}$$

Using Eqs. (3.4)-(3.6) and Eq. (3.9) in Eq. (3.3) we get

$$\begin{bmatrix} G_2(s) \\ F_3(s) \end{bmatrix} = \mathbf{HT}\left[\mathbf{RT} + \mathbf{\Pi}\right]\begin{bmatrix} G_2(s) \\ F_3(s) \end{bmatrix} , \tag{3.10}$$

and subtracting the right side of Eq. (3.10) yields the overall representation of the system

$$\mathbf{M}\begin{bmatrix} G_2(s) \\ F_3(s) \end{bmatrix} = 0, \quad \mathbf{M} = \mathbf{I}^{2\times 2} - \mathbf{HT}\left[\mathbf{RT} + \mathbf{\Pi}\right] , \tag{3.11}$$

with $\mathbf{M}$ being the entire system matrix. Such a description allows for stability analysis via classical eigenvalue examination. The characteristic equation given by determinant of $\mathbf{M}$ is a quasi-polynomial equation involving time delays. Upon the assumption of linearity and time invariance of the heater transfer function $\mathbf{H}$, such dynamics are called Linear Time-Invariant Multiple Time-Delayed System of Neutral type (LTI-NMTDS), for which there has been a theory developed in recent years for analyzing the stability. It is hence possible to use the concept for controller design and optimizing plant design, in terms of adjusting the time delays by changing the position of the elements in the tube. This methodology is presented in [9, 6] and involves a Quasi-Polynomial mapping based Root finder (QPmR) method for finding the roots, which is developed by Vyhlídal and Zítek [15] and Cluster Treatment for Characteristic Roots (CTCR) paradigm for generating the stability maps.

In this work, rather than focusing on the stability analysis, I am concerned with the oscillation performance and their evolution in time and as stated in Section 3.1 already, assumptions of linearity and time invariance of $\mathbf{H}$ are invalid in such case. In the following chapter, modeling of the heat transfer is described, including the nonlinear time varying-character.

3.3 Velocity-Dependent Heat Transfer

During experiments with a physical Rijke tube platform, we observe two distinct phenomena which are in strict conflict with the LTI-NMTDS description. First, there are the dynamics of the buoyancy-induced convection flow, which has varying influence on the acoustic performance, depending on the size and form factor of the tube as well as the external parameters and disturbances such as the temperature and motion of the surrounding air. Second, there is a limit cycle behavior and saturation in the amplitude observed in the measured acoustic pressure, whereas in a linear system, the expected response is harmonic and for positive heat release performance gain that overweights the losses on the reflections, the amplitude of the induced oscillations grows exponentially. Therefore, in order to obtain a model that can be practically useful for time-domain simulations, I need to drop the assumption of stable mean convection flow and consider nonlinear parameter-varying system instead.

Let me first introduce the linearized version of the heater transfer function

$$\mathbf{H}(s) = \frac{1}{s + Z_1 + Z_2} \begin{bmatrix} Z_1 & s + Z_1 \\ s + 2Z_1 + Z_2 & -Z_1 \end{bmatrix} , \tag{3.12}$$

with the coefficients

$$Z_1 = \frac{a(\gamma - 1)}{2Ab\bar{c}^2\bar{\rho}} \quad \text{and} \quad Z_2 = \frac{1}{b} , \tag{3.13}$$

where b is the time constant of the heat release dynamics, a corresponds to its DC gain, A is the cross-sectional tube area and γ is the adiabatic ratio. Eq. (3.12) is borrowed from the development in [9, 6] and the form of coefficients in Eq. (3.13) are broadly accepted in other relevant sources [3, 2]. The core elements to the heat transfer are the effective heat gain represented by a and then first-order lag dynamics based on the boundary-layer effect of thermal inertia [2].

In the cited references which employ Linear Time-Invariant (LTI) system theory [9, 3, 6, 2], the heat release gain a is considered proportional to the heat power transfer Q of a hot circular wire in a colder fluid, which is approximately given by King's law

$$Q = l_\mathrm{w} \left(\kappa + \kappa_u \sqrt{|u_\mathrm{h}(t)|} \right) (T_\mathrm{w} - T_\mathrm{gas}) , \tag{3.14}$$

where l_w is the length of the heater wire, κ is the fluid's thermal conductivity, κ_u is an empirically determined constant and $u_\mathrm{h}(t)$ is the velocity of the gas at the heater cross section [17]. Assuming the wire temperature T_w and gas temperature T_gas as well as the mean flow velocity to be constant and velocity fluctuations small renders Q and a respectively to be constant as well.

Dropping the assumptions results in a becoming a time-varying parameter $a(t)$ as a nonlinear function of the velocity and possibly also a linear function of wire and gas temperature. Moreover, the wire temperature T_w is also influenced by the velocity of the gas, rendering that variable a likely major contributor to the nonlinear behavior. Based on this reasoning, I decided to neglect the other dependencies (such as the overall temperature increase over time as the tube itself absorbs the heat) and only consider the heat release gain to be

$$a(t) \propto Q(u_\mathrm{h},\Delta T_\mathrm{w}) = C_1 \left(1 + C_2\sqrt{|u_\mathrm{h}(t)|}\right) \Delta T_\mathrm{w}(t)\,, \tag{3.15}$$

where $\Delta T_\mathrm{w}(t) = T_\mathrm{w}(t) - T_\mathrm{gas}$ is relative temperature of the wire w.r.t. the temperature of the surrounding gas and environment, which I consider as a constant reference point, and $C_1 = l_\mathrm{w}\kappa$ and $C_2 = \kappa_u/\kappa$ are constants. This relative temperature is proportional to the energy which is the integral of the difference of electrical power supplied to the wire and the heat power transferred to the flowing air, hence

$$\Delta T_\mathrm{w}(t) \propto E_\mathrm{w} = \int R(T_\mathrm{w}) i(t)^2 - Q(u_\mathrm{h},\Delta T_\mathrm{w}) dt\,, \tag{3.16}$$

with $i(t)$ being electrical current flowing through the wire and $R(T_\mathrm{w})$ the electrical resistance of the wire. For the sake of simplicity I neglect the temperature dependency of the wire resistance, hence $R(T_\mathrm{w}) = R$ is constant. Next, using Eq. (3.15) in Eq. (3.16), adding the proportionality constant C_3 and differentiating the result, I obtain an affine first order differential equation for ΔT_w with nonlinear time-varying terms in $i(t)$ and $u(t,x_0)$

$$\Delta\dot{T}_\mathrm{w}(t) = -C_3 \left[C_1 \left(1 + C_2\sqrt{|u_\mathrm{h}(t)|}\right) \Delta T_\mathrm{w}(t) - R i(t)^2\right]\,. \tag{3.17}$$

The equation Eq. (3.17) describes the dynamics of the wire temperature with the current $i(t)$ being the control input to the system. The time-varying heat transfer gain can then be written as $a(t) = C_a Q(t)$, where $Q(t)$ is influenced by $i(t)$ and the dynamically changing relative wire temperature $\Delta T_\mathrm{w}(t)$. Figure 3.2 shows the block diagram implementation of this dynamics as it is later used in the complete model.

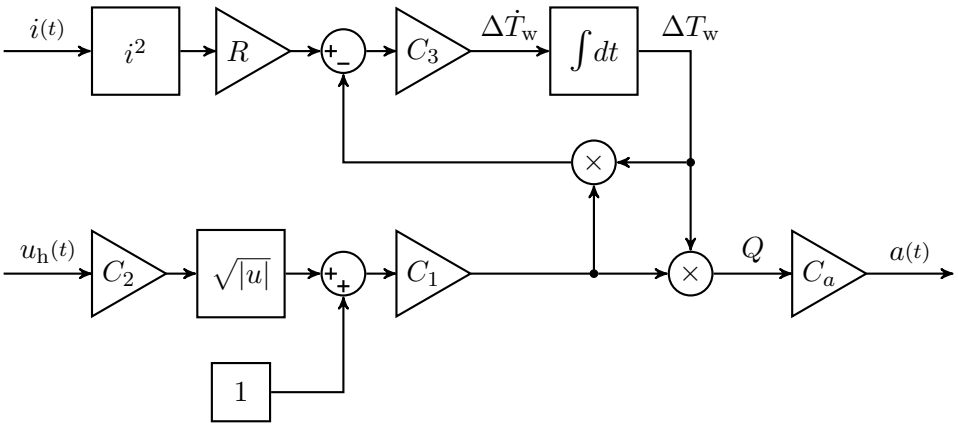

Figure 3.2: Block diagram of the time-varying heat transfer gain model.

3.4 Buoyancy-induced flow dynamics

The velocity $u_\mathrm{h}(t)$ is given by acoustic velocity fluctuations $\tilde{u}(x_0,t)$ at the heater cross section and the velocity $u_\mathrm{b}(t)$ of the buoyancy-induced convection flow, such that

$$u_\mathrm{h}(t) = \tilde{u}(x_0,t) + u_\mathrm{b}(t)\,. \tag{3.18}$$

In order to model the time-domain character of the system, including the attack and decay of the acoustic instabilities, it is important to consider the dynamics

of $u_{\mathrm{b}}(t)$. Assumed low velocity compared to the velocity of the sound does render changes in this airflow negligible w.r.t. to the acoustic part of the dynamics, however, the effects on the heat transfer are considerable.

The acoustic velocity fluctuations are easy to obtain from Eq. (3.2), given the knowledge of the functions $f(t-x_0/\bar{c})$ and $g(t-x_0/\bar{c})$, which I can directly obtain from the simulation model based on the diagram in Figure 3.1b, yet the convection flow component requires its own model. Several different approaches to modeling of the convection flow in the straight heated pipe are compared in [18], ranging from an over-simplified 1D model to the full Navier-Stokes. However, these models are asymptotic (focusing on the steady state flow), hence not useful for simulating the transients. Considering the approximations and simplifying assumptions that were already applied to the previous components of the model, I decided against complex derivations of the fluid dynamics using Navier-Stokes. Instead, I approximate the behavior using a simple 2nd order system, representing some virtual inertia m of the air column and damping ζ caused by viscous friction in the tube and even more so the damping effects at the tube ends.

$$C_a a(t) = m\dot{u}_{\mathrm{b}}(t) + \zeta u_{\mathrm{b}}(t)\,. \tag{3.19}$$

The input to the system is the heat release gain $a(t)$ and it is scaled by a constant C_a. The virtual inertia m is proportional to the inner volume of the tube and the friction coefficient f is assumed constant. Numerical values of all the parameters are empirically determined based on model experiments such that the system reaches reasonable steady-state velocities ($u_{\mathrm{b}}(t) \approx 1\,\mathrm{ms}^{-1}$) for given input current and consequent heat release gain. Eq. (3.19) yields a simple transfer function

$$H_{\mathrm{b}}(s) = \frac{C_{\mathrm{b}}}{ms+\zeta}\,, \tag{3.20}$$

which can be implemented in the model of the time-varying heat gain model as shown in Figure 3.3

To summarize, the final form of the transfer function $\mathbf{H}_a(s)$ remains identical to the LTI model, only its parameter $a(t)$ is now time-varying and it is governed by the equation $a(t) = C_4 Q(t)$, where $Q(t)$ is influenced by the electrical current $i(t)$ and the dynamically changing velocity $u_{\mathrm{h}}(t)$ via the relative wire temperature $\Delta T_{\mathrm{w}}(t)$. Simplified block diagram of such a system is in Figure 3.3. I selected constants C_1, C_2, C_3, C_4 and C_a based on the empirical observation of real heater and tube. Due to the coupling effects of several different dynamical models, and a lack of precise dynamical measurements of the temperature and airflow, there is no simple and secure way of system identification.

3.5 Reflection Coefficient

I introduced the physical essence of the reflections at the end of the tube in Section 2.1 and pointed out earlier in this chapter the discrepancy of the model from [9] which I used as a conceptual foundation. Despite the misleading term *coefficient*, the reflection coefficient is a function of complex frequency. Ideally, it would be represented by a filter transfer function which would provide variable frequency gain and specific phase delay.

The reflection coefficient formula in Eq. (2.1) corresponds to a form of a linear phase filter. Such filter delays each frequency component of the signal by the same

fixed amount commonly referred to as a group delay. Linear phase Low-Pass filters can be designed using Finite Impulse Response (FIR) filter method or using a Bessel filter design, but achieving the proper desired shape of the magnitude response is difficult, if feasible, and would likely yield higher order filter and undesirable complication of the model [19]. To avoid the complexity, I decided to model the reflection by a simple gain $-|R_\mathrm{r}|$ and a 1st order Low-Pass filter with a cutoff frequency at $10f_0$. Such implementation may deviate from the physical reality slightly, mainly because the phase response is not linear, but the most important aspect regarding the attenuation of the higher frequencies is included.

The frequency that is considered for computation of $|R_\mathrm{r}|$ as in Eq. (2.2) is the fundamental resonant frequency of the tube, closely approximated by $f_0 = \bar{c}\,l/2$. I also adjust the formula for Helmholtz number to

$$ka = \frac{1.5\pi r}{2l} = \frac{1.5\pi r f_0}{\bar{c}}\ , \tag{3.21}$$

The constant 1.5 in the numerator of Eq. (3.21) was added to decrease the magnitude of the reflection coefficient artificially. As such, the energy losses represented by the coefficient account for other means of energy dissipation, which I do not model directly. The value is purely empirical and does not heavily influence the qualitative behavior of the model. For given tube radius and tube length $l_\mathrm{t} = 0.5\,\mathrm{m}$, yielding a frequency $f_0 = 328\,\mathrm{Hz}$ the value of $|R_\mathrm{r}| \approx 0.935$ closely matches the value used in [9] for modeling a tube with nearly identical dimensions.

3.6 Microphone Placement

Review of literature which deals with physical Rijke tube or more general ducted flame experiments that incorporate a single sensor of acoustic pressure [8, 3, 2, 6] reveals that the sensor placement is uniformly chosen in the downstream section of the tube. Epperlein explains in [2] that the microphone position generally influences only the locations of the zeros of the system, and, therefore, affects the observability of the system modes. Such a fact does not come as a surprise when the physical principle of the system is considered. If the sensor is placed to a position which collocates with an acoustic node of a given mode of a sound wave in the tube, such a mode does not contribute to the measured signal. Based on this reasoning, a typical sensor placement is near the downstream end of the tube, sufficiently far

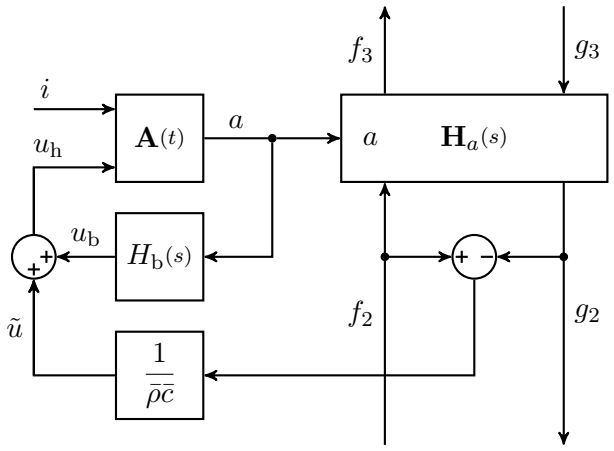

Figure 3.3: Block diagram of the parameter-varying heat transfer model.

inside of the tub, so it avoids undesirably high attenuation of the lower acoustic modes. In fact, even the placement at the very end of the tube usually provides sufficient measurement, due to the end correction discussed in Section 2.1.

Motivated by the simplicity of the design for the Rijke tube organ, I decided to experiment with the microphone at the opposite (bottom) end of the tube, in the upstream section. Schematic drawing and a block diagram representing such setup are in Figure 3.4. The practicality of such setup is further justified in Section 6.4. Note that the values of τ_i now correspond to different physical distances. For this new microphone placement $\tau_1 = (x_\mathrm{u} - x_\mathrm{m,u})/\bar{c}$, $\tau_2 = x_\mathrm{m,u}/\bar{c}$ and $\tau_3 = x_\mathrm{d}/\bar{c}$.

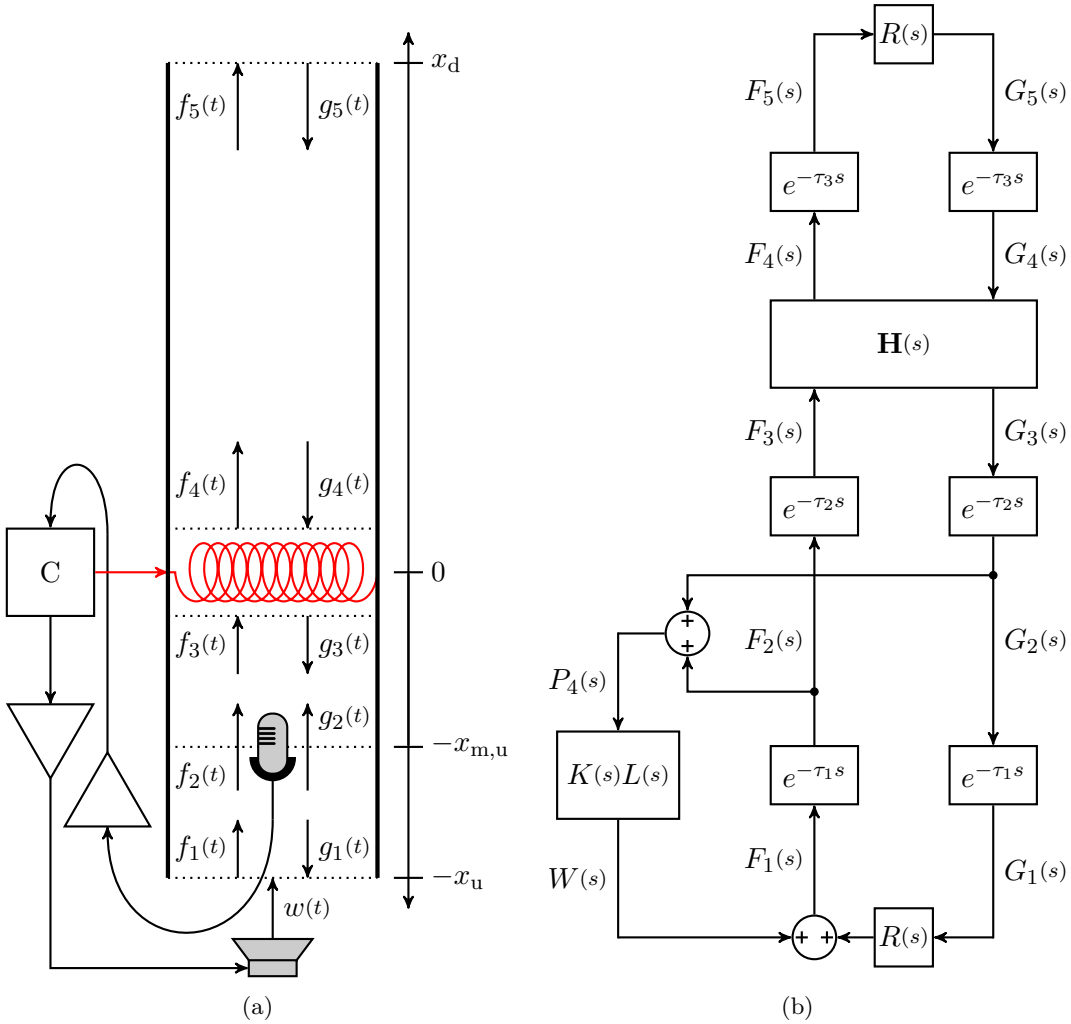

Figure 3.4: Schematic (a) and block diagram (b) representation of the simplified time-delay based model of the Rijke tube with upstream microphone placement.

In a plain resonant pipe without a heat source and convection, the measurement on both ends should be symmetrical. In a Rijke tube, however, the additional effects render both placements different, as the limit cycle projects differently to the wave behavior below and above the heater. The difference in measured signal is apparent in Figure 3.5 and similarly in the simulated outputs from both models in Figure 3.8

There are several aspects to consider when comparing the two placements concerning the microphone performance in the control architecture and drawing direct conclusions without extensive experimentation and testing is difficult. First, there

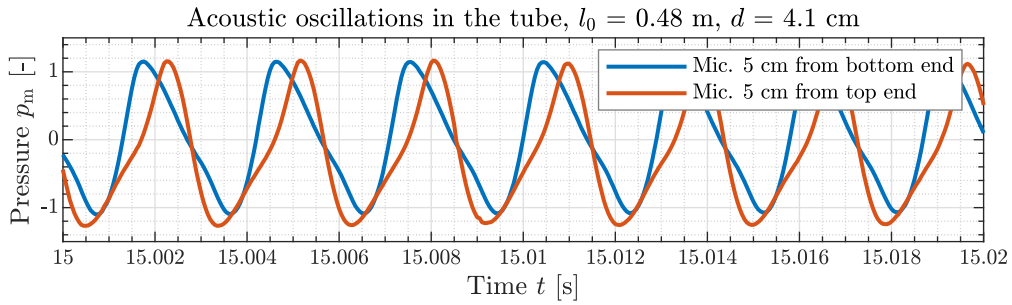

Figure 3.5: Comparison of the measured signal from the tube for upstream and downstream microphone placement.

is certainly a stronger gain of the transfer function from the loudspeaker to the microphone signal, caused simply by the closer proximity of the two components. In extreme case, this effect equals to a delayed feed-through in the system and consequent propagation of the control signal $w(t)$ to the feedback. Should it prove detrimental to the performance of the control system, this issue can me mitigated by identifying the feed-through constant and time delay and subtracting the input signal from the measured output. Interestingly, this issue appears in the derivation of the model description, when computing the feedback controlled signal for the downstream placement topology in Figure 3.4b. Equivalently to the Eq. (3.7), I get

$$W(s) = K(s)L(s)\left(F_2(s) + G_2(s)\right) , \tag{3.22}$$

which can be expanded as

$$W(s) = K(s)L(s)\left(e^{-\tau_2 s}G_3(s) + e^{-(2\tau_1+\tau_2)s}R(s)G_3(s) + e^{-\tau_1 s}W(s)\right) , \tag{3.23}$$

$$W(s) = \frac{K(s)L(s)e^{-\tau_2 s}\left(1 + e^{-2\tau_1 s}R(s)\right)G_3(s)}{1 - K(s)L(s)e^{-\tau_1 s}} . \tag{3.24}$$

Clearly, the expression is more complicated when compared to Eq. (3.8) featuring a delay term in the denominator. In-depth QPmR based analysis of the impact of such change on the stability regions is beyond the scope of this work, but this is an interesting result, and it may warrant a closer inspection in the future work. For the purposes of this development, I relied upon experimental results from both the simulation model and the physical apparatus to prove that the upstream microphone placement has little to no detrimental effect on the abilities of the control system.

3.7 Model Validation and Experiments

I assembled all the components described in the previous sections into a MATLAB® Simulink® model and tested for different physical parameters of the tube. Given the unusual nature of the model which contains a loop of time delays as a core feature and source of the observed dynamics, I was not able to rely on some existing modeling tools. Several details regarding the implementation are in Section 3.8, Numerical values of some of the constants in the model are adjusted, so the resulting signals approximately correspond the measurements on the physical apparatus. For the values of unmeasured quantities (e.g., the velocity u_b of the buoyancy flow or the variable wire temperature T_w) I empirically determined the bounds. It is important to emphasize that this model does not aim for the absolute quantitative accuracy, as

if it was meant to be used for state estimation. My objective was to capture within the model the essence of some of the noteworthy aspects of the Rijke tube dynamics.

The first set of experiments I conducted were system responses to small sound pressure initial condition. At the time $t = 0$ the relative heater temperature is 0 °C, and there is no buoyancy flow. There are no crafted signals entering the model which would carry the tube's resonant frequency, and the active sound control input $w(t)$ is zero. The input current to the heater is set to 2.3 A, a value corresponding to the maximum input current to the heater in the experimental setup, which is described in Chapter 4. Plots of the simulation results are in Figure 3.6, showing the development of sound pressure p_{m} at the microphone cross section, relative wire temperature ΔT_{w}, the velocity u_{b} of the buoyancy induced airflow and the acoustic velocity u_{h} at the heater section.

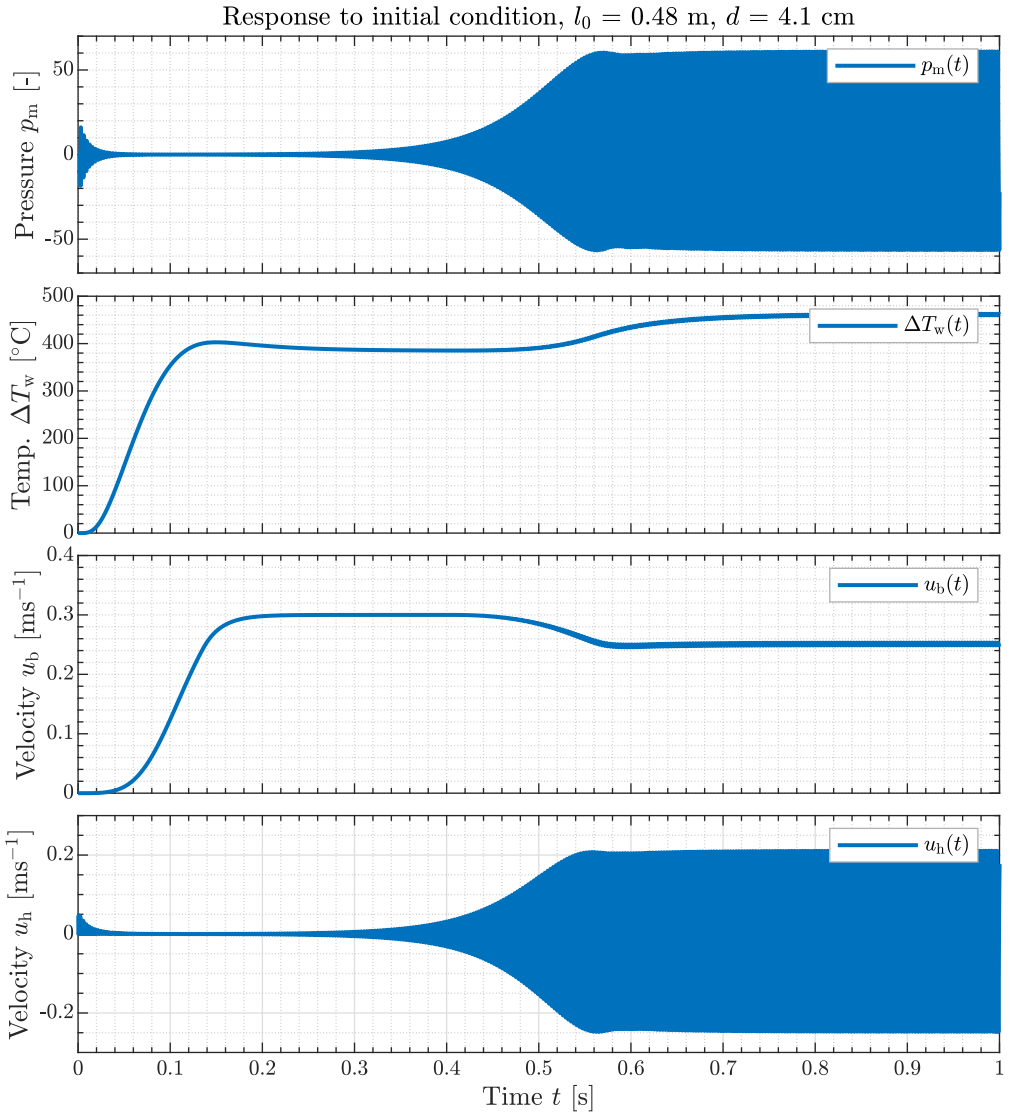

Figure 3.6: Tube model response to small initial sound pressure disturbance.

.

The transients of the temperature and the buoyancy flow correspond with the expected behavior. The rise of heater temperature consequently induces the buoy-

ancy flow, which then in response slows down and eventually overturns the heating. Combination of higher temperature and mean flow eventually yields high enough heat transfer gain that the pressure and velocity oscillations in the tube start to strengthen, up to a point where the gain stabilizes.

The Fast Fourier Transform (FFT) analyzed frequency spectrum of the sound pressure signal plotted in Figure 3.7 confirms that the system oscillates at the frequency closely matching the expected frequency f_0 determined by corrected length of the tube l. The presence of lower gain higher harmonic components in the spectrum also complies with the expectation.

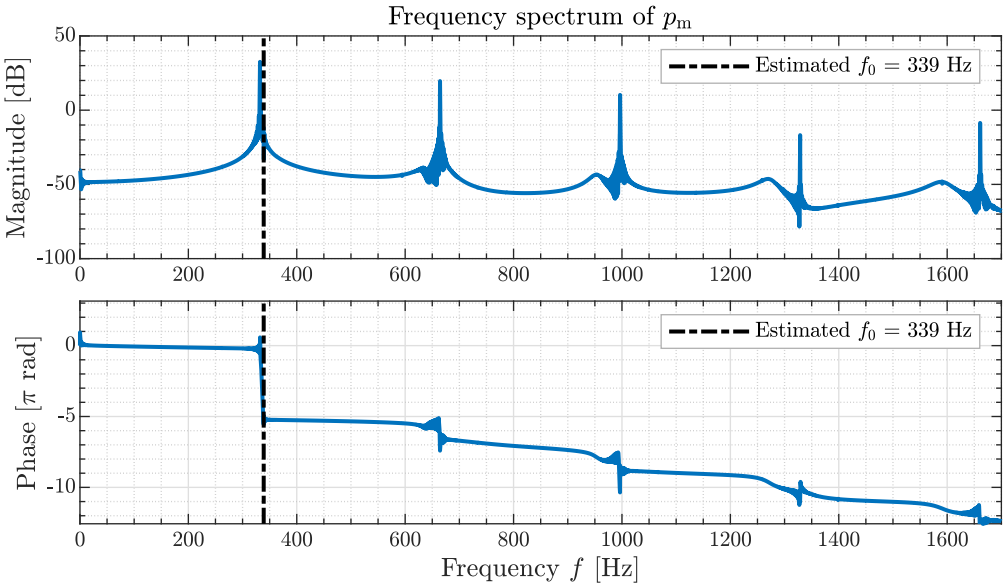

Figure 3.7: Frequency spectrum of the sound pressure signal.

Figure 3.8 shows the comparison of 20 ms long time samples of the sound pressure signals for Rijke tube models with upstream and downstream microphone placements. The shape of both signals almost perfectly matches the observation from the experiment with real Rijke tube shown in Figure 3.5. It is worth noting, however, that while the model response features fully saturated amplitude, the signal from the real-life experiment corresponds to a lower than maximum amplitude.

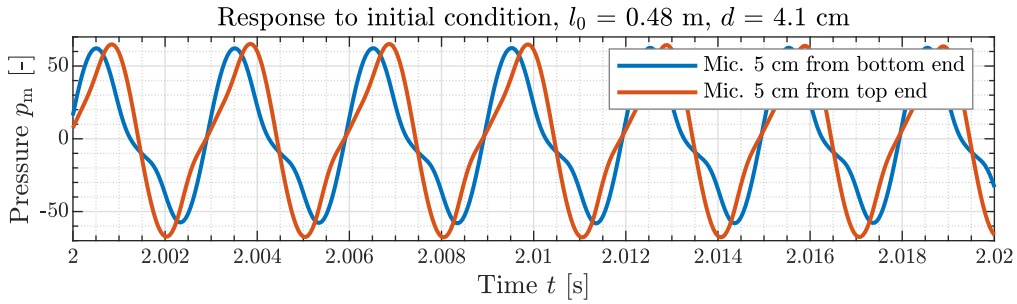

Figure 3.8: Comparison of the simulated model sound pressure for upstream and downstream microphone placement.

The influence of the input current to the heater is illustrated in Figure 3.9, featuring a notably slower rise of the oscillations for lower current $i = 2$ A. Increased

length of the tube and constant current yield similar outcome, as shown in Figure 3.10. Here the difference in the rise is even more prominent.

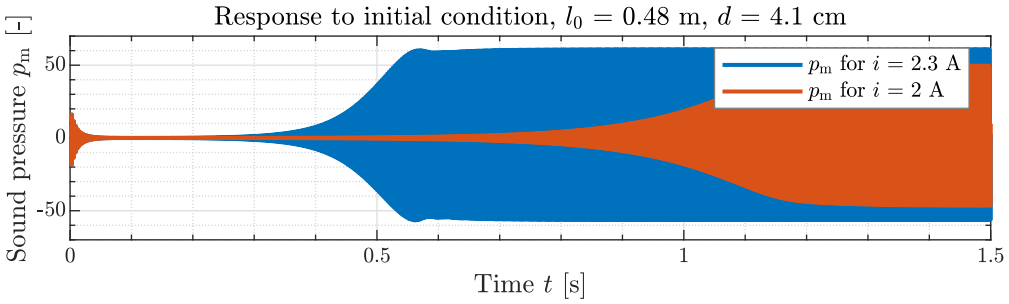

Figure 3.9: Difference in model responses to initial condition for different values of heater current.

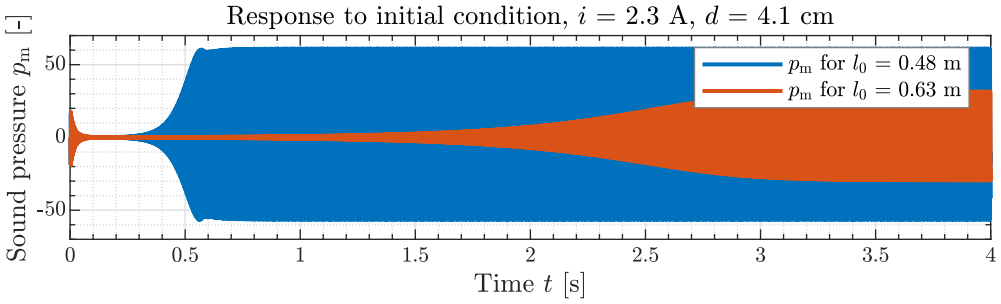

Figure 3.10: Difference in model responses to initial condition for different lengths of the tube.

More experiments performed on the model can be found in Chapter 5, where I describe and test the two distinct control systems and further discuss the quality of the match between the model and physical Rijke tube.

3.8 MTD Model Implementation in MATLAB® Simulink®

In the domain of linear time-delay system, there has been recent development which utilizes Linear Fractional Transformation (LFT) to represent the system, and there is a working functionality implemented in Control System Toolbox in MATLAB® [20]. This framework provides methods for simulation, analysis, and control of generalized LTI systems, including those with delays in the feedback path. However, it is not currently suited for Linear Time-Varying (LTV) or Linear Parameter-Varying (LPV) systems and, therefore, not readily applicable for my purpose.

Instead of opting for approximations, I attempted to simulate the model purely using a Simulink® diagram that corresponds to the model in Figure 3.4b extended with the nonlinear dynamics in Figure 3.2. I feared possible issues and erratic behavior caused by cumulative errors in the time-delay loop. Surprisingly, the simulation executes as expected and the model seems reasonably robust to parameter variations. For varying physical parameters of the simulated tube, it is important to properly adjust the heater gain constant C_a, where a value too low causes the system to be stable and a value too high prevents the nonlinear dynamics from saturating the oscillations, which then grow exponentially. Another highly influential parameters which need to be empirically adjusted are the buoyancy flow gain constant C_b and

damping ζ. Increased sensitivity to these parameters suggest that the model of the airflow is indeed the weak link of the overall structure and it could be improved upon.

4 | Prototype Platform

Prior to designing a larger scale organ-like platform consisting of multiple Rijke tubes, I built a prototype testing rig with one tube to run experiments and use the results to later determine some important design decisions. In particular, I experimented with the design of the heating element, the loudspeaker and microphone placement and specifications and the overall acoustic performance and limits of the setup.

The prototype tube stand in Figure 4.1b is a simple design that employs a 3D-printed foot that screws down to the base and holds a standard 20×20 mm aluminum extrusion, which allows a split ring shaped 3D-printed tube clamp and heater holder to be mounted in arbitrary height. The last fabricated component is a simple holder for the loudspeaker. Provided an access to 3D printer, such setup is very quick, easy, and relatively cheap to make. Moreover with a sufficiently rigid base it is surprisingly sturdy and works with larger tubes as well.

The initial tests and experiments conducted to prove the concept of feed forward impulse as a mean of accelerating the attack of the thermoacoustic instability in the tube were performed on the Rijke tube platform built by my colleague student Lukáš Černý in [21], which is shown in Figure 4.1a. With a tube length $L = 1310$ mm and a diameter $d = 85$ mm this apparatus is significantly larger than my next prototype platform featuring a tube with $l_0 = 483$ mm and $d = 41$ mm, rendering the internal volume of the tube almost $12\times$ smaller when compared to the larger setup.

Being able to compare the performance of the two different sizes of Rijke tube helped to identify the difference of the robustness of the internal tube dynamics against external disturbances, caused by the changes of temperature and motion of the surrounding air, with the larger tube being much less prone to deviations in the amplitude of the sound, when compared to the smaller tube, which is easy to completely inhibit from oscillating just by inducing a blow of air around the top end of the tube.

Conversely there is a different parasite property associated with the larger tube, caused by the thicker and more massive tube walls. These have much larger heat capacity and it turns out that for longer duration of experiments with the heating turned on, the glass eventually warms up in the large section above and below the heater, which in pair with a slower buoyancy airflow in the larger tube disrupts the property of spatially isolated heating region. Consequent temperature and pressure gradient in the tube is lower, hence the conditions for the thermoacoustic instability are impaired. In some experiments, this eventually disabled the instability from occurring in the larger tube, and it was necessary to let the tube walls cool down in order to re-initiate the proper conditions.

Despite being quite intuitive and easy understand, neither of these properties seem to be documented in the related literature. Possible reason in that there has been little to no scientific interest in the actual acoustic performance of the Rijke

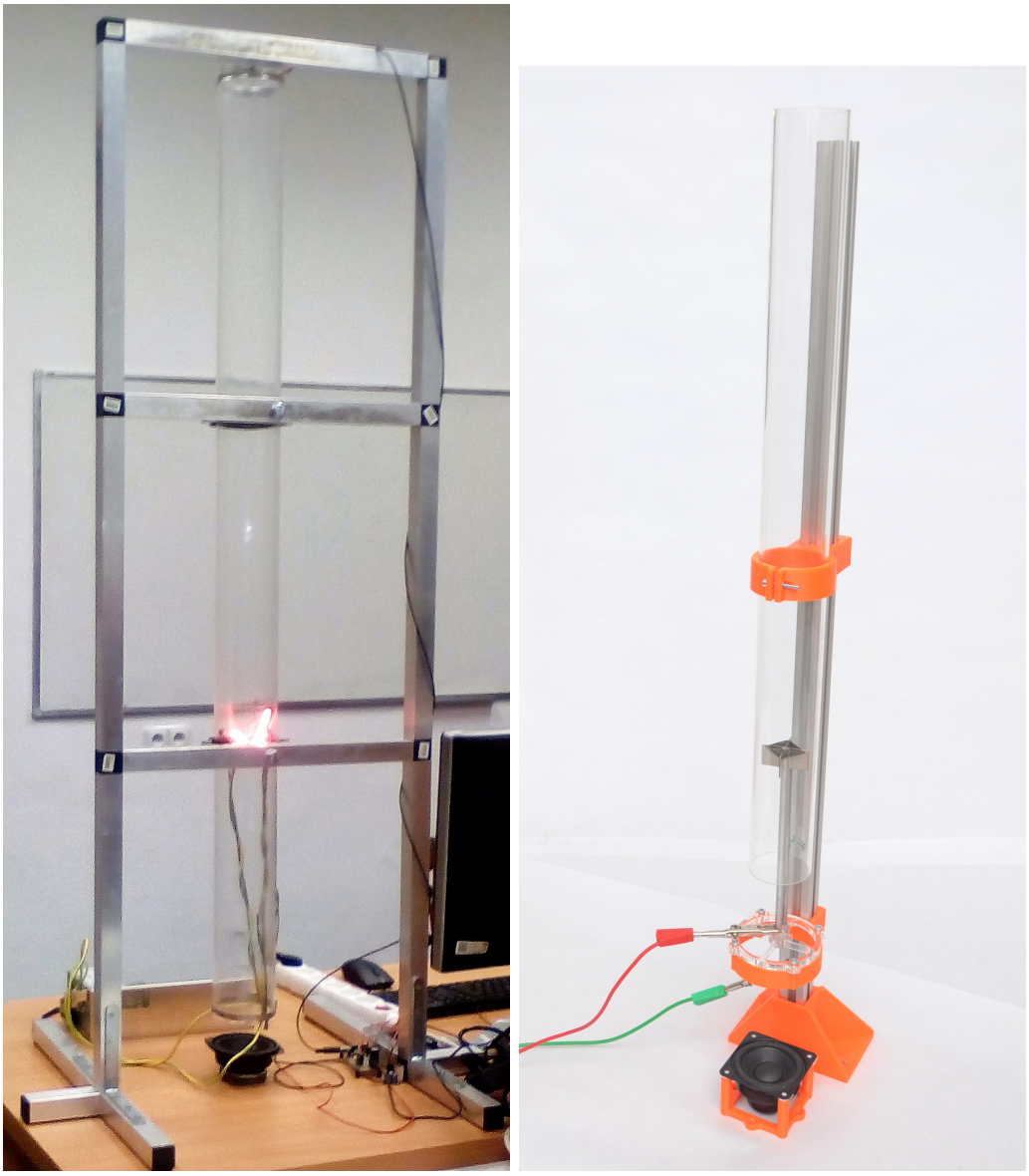

(a) (b)

Figure 4.1: Photographs of Rijke tube apparatus built by Lukáš Černý (a) and my prototype setup (b).

tube concerning its use as a musical instrument. In my development, I address both issues in Section 5.2 in the design of the control scheme using the heater power as an control input to both stabilize the amplitude of the sound and to prevent the tube from heating up prohobitively.

4.1 Heater Design

In the experiment leading to his famous discovery, Rijke used a wire-gauze made of 0.2 mm diameter iron wire placed inside the tube, which he brought to red heat by a hydrogen burner lamp. This method is certainly has its charm and is still being used nowadays for simple, yet effective Rijke tube demonstrations. For any more permanent experimental setup, electrically powered heating coils are used almost

exclusively, bringing higher convenience and options for regulating the heater power output. In published literature, researchers rarely put high emphasis on the actual design of the heating coil. Usually, it is only re-iterated that the wire has to be sufficiently long and the formed coil should not be extending over a long region in the tube lengthwise. Often, the coil is simply suspended from the top and its wire leads are directed down, out of the bottom end of the tube. I found only two cases of more advanced designs, both of which are associated with the two existing attempts on building Rijke tube organ which I mention in Chapter 1.

Both designs suspend the heater from the bottom, using either single alumina tube[1] to run the lead wires through, or a pair of aluminum rods to act as both structural support and an electrical lead, and also provide very flat heater bodies, which is in good compliance with the assumption of narrow heating region stated in Section 3.2.

Second design seems to take inspiration in heater elements found in commonly available products, such as hair dryers and small electric stoves, which uses a wire coil wound through a thermally and electrically insulating structure usually made out of laminated mica plates.

I decided to take an inspiration in the second mentioned design, as it is more substantial and seems to be more easily reproducible in larger quantity. The heater includes a cross consisting of two plates made out of rigid silicone-bonded muscovite mica plate. This material has excellent properties for this use, including heat resistance up to 900 °C and electrical insulation resistance of more than $10^{12}\,\Omega \cdot \mathrm{cm}$ at 500 °C. The downside of this material is its tendency to turn into flakes upon cutting, although the severity of this property may vary with the quality of the product. The mica cross is seated in the cross shaped slot on top of one of the aluminum rods, and there are equally spaced parallel slots cut into the top facing edges of the cross, which accept the winding of the wire. I used a 0.5 mm slitting saw mounted in the vertical milling machine to cut these slots, mainly to avoid flaking and also to obtain accurate and narrow slots. The second aluminum rod has a simple slot and it accepts one of the ends of the mica cross. The heater wire I used is 1 mm wide 0.05 mm thick Kanthal[2] A1 type resistance wire and it is pressed into the cross shaped slot in the center aluminum rod and then wound outwards through the small slots in the mica plates. The end of the winding is again pressed into the slot in the other aluminum rod. The photographs of the prototype heater are shown in Figure 4.2.

Including the aluminum lead rods, this heater has a resistance of $\approx 14\,\Omega$ and connected to a 30 V laboratory DC power source, it outputs around 65 W of heating power. I observed the drop in the drawn current as the wire heats up and the ratio between the maximum value $i_{\max}$ at the beginning and the minimum value $i_{\min}$ with the wire fully heated yielded

$$C_{\mathrm{t}} = \frac{i_{\max}}{i_{\min}} = \frac{2.3}{2.2} = 1.04\bar{5}\,, \tag{4.1}$$

which, assuming that the maximum measurement corresponds to the wire at room temperature, gives an estimate of the peak temperature to around 700 °C. The uncertainty of this estimate is no better than ±50 °C because of the error in the current measurement and also the accuracy of used conversion chart.

[1] Aluminum oxide (Al_2O_3), a non conductive mineral based material.

[2] FeCrAl alloy resistant to oxidizing and corrosion, offering higher maximum operating temperature than Nichrome wire. The specific product that I used is made by Crazy Wire company (www.wireandstuff.co.uk)

The constructed heater provides satisfactory performance, as it outputs enough heat to drive the acoustic instability in the tube at the reasonable draw of electrical power. Thanks to the low volume of the wire, it is also very fast to heat up and cool down, which is beneficial for further attempts of control. The downside of this heater construction is the complicated fabrication, involving extremely tedious cutting of the slots in the mica plates, and also limited adjustability of the length of the aluminum lead rods once the heater is completed. Given that the exact position of the heater in the tubes of different lengths may be a subject of tuning, it would be useful to have a unified size of the heater element along with some adjustable or interchangable lead rods. The last issue with this particular design is the tendency of the wire to raise up from the slots due to the thermal expansion during the heat-up, causing the risk of shortage between the adjacent wire loops and consequent burn-through. I addressed all of these issues in the updated heater design described in Section 6.3.

4.2 Sensor and Actuator

Both selecting and mounting a microphone and a loudspeaker to achieve satisfactory performance of the active control system are non-trivial tasks, especially if practicality and affordability is also involved. From the early start I considered the feasibility for multiplication of given setup and also its versatility concerning different tube sizes. The microphone in particular should be small enough not to obstruct the airflow and spoil the end reflection in smaller diameter tubes. For the prototype platform I reused the same microphone setup that was used in [21], which relies upon very cheap 9×4.5 mm electret condenser microphone cartridge, which is often used for PCB mount applications, and placed it near the top end of the tube to mimic virtually all of the other documented setups with a Rijke tube. The eventual change in design and placement of the microphone sensor mentioned in Section 3.6 was only made during the design of the complete organ, which is described in Chapter 6.

For the loudspeaker, I was experimented with smaller universal speakers of several sizes and respective maximum power outputs ranging from 5 W to 15 W. Quickly appearing problem with such speakers is not only the insufficient power for successful stabilization of loudly humming tube, but also unpleasantly distorted

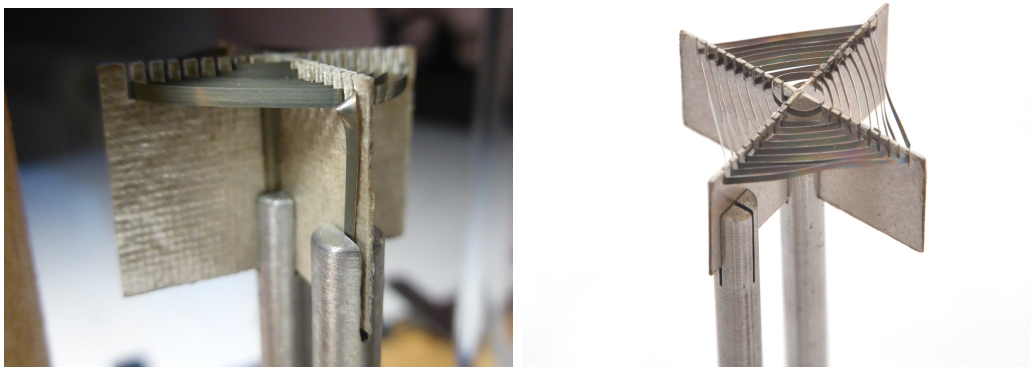

(a) (b)

Figure 4.2: Photographs of the inspiring design (a) and constructed prototype (b) of the heater element.

sound that they produce during these attempts. I eventually transitioned towards larger loudspeaker, which eventually motivated a conceptual change to the design of the organ described in Section 6.1.

5 | Control System

It has been shown that it is possible to actively stabilize the Rijke tube in terms of successful suppression of the unstable acoustic oscillations [12, 2, 3, 6, 8, 22] and even passively influence the unstable poles of the system by enhancing the tube with a Helmholtz resonator [9]. However, I did not find any documented attempts on automated control system aiming on improving the acousic performance of the Rijke tube. All of the existing attempts I was able to find,that brought Rijke tube to the domain of musical instruments, only involved manual operation.

In Section 5.1 I form several requirements and goals for the control system which I then develop in Section 5.2 and Section 5.3, and test both on the mathematical model and the real apparatus. Most of the real experiments were performed on the prototype platform described in Chapter 4, except for the attempts for multi-modal control, which required the full platform with multiple operating Rijke tubes.

There are several approaches to modeling of the simplified Rijke tube system. Given its numerous nonlinear aspects it depends on the purpose of the mathematical model whether a linearization or straightforward neglection is acceptable. In this chapter, I first present and discuss various approaches with respect to the related developments as well as this work, offer some justification to the consequent choices I made and finally derive a model which is later used for experiments and control design.

5.1 Control Requirements

In order to improve the performance of a Rijke tube as a musical instrument, several of its inherent qualities need to be enhanced. An amplitude regulation is required in order to, (i) provide steady tone, mittigating the detrimental influence of the buoyancy flow and external flow disturbances, and (ii) to allow playing the tone at different sound levels. With sufficient heat input and no regulation, Rijke tube typically saturates on its maximum aomplitude, which features the most prominent disharmonic limit cycle sound. Hence, being able to regulate the amplitude down may also result in more sine-like oscillation and better quality of tone.

Next requirement targets the acceleration of rise and decay of the sound (iii). In uncontrolled tube, these dynamic transients get slower with increasing size of the tube, and lack consistency, which prevents precise triggering of faster notes. Rise in particular is very sensitive to initial conditions, including the temperature profile along the tube and the initial airflow, hence conditions which can not be easily adjusted and repeated.

Both heater input current control and acoustic control via loudspeaker may contribute towards all of the requirements, yet there is one aspect regarding the acoustic control that I want to emphasize. From the perspective of the Rijke tube as an exotic musical instrument, it seems undesirable to have some continuous audible

loudspeaker action contributing to the overall sound profile of the device. It might be possible to allow such operation by designing the platform in a way that the sound from the loudspeaker is better contained within the device and only affects the pressure inside the tube, but I did not consider conducting experiments in that direction. Existing open design of the device allows the sound from the loudspeaker to propagate and inevitably mix with the sound from the tube, and as such possibly spoil the overall impression. In order to prevent that, I actively tried to limit the lloudspeaker action.

This decision essentially excludes the loudspeaker input from some longer term amplitude control, where a continuous signal of nonzero amplitude would be required. However, during the task of active feedback suppression of the sound in the tube, the output from the loudspeaker should be close to zero except for the transient prior to the stabilization. Moreover, for the active feed forward initiation of the sound, it is possible that even a short impulse low in amplitude will be sufficient for the acceleration of the tone rise. This qualifies the acoustic feedback for control tasks associated with the third requirement.

5.2 Heater Control

Except for the limit case of zero amplitude, hence a complete sound suppression, the sound level is only regulated by controlling the input current. The control scheme is a simple feedback loop illustrated in Figure 5.1

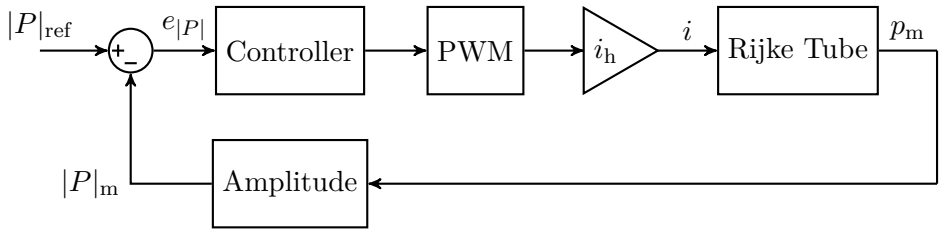

Figure 5.1: Block diagram of the amplitude control system.

I assume the acoustic signal to be close enough to harmonic and define the sound amplitude $|P|$ as

$$|P| = \sqrt{\frac{2}{T}\int_{t_0}^{t_0+T} [p_{\mathrm{m}}(t)]^2\, dt}\,, \tag{5.1}$$

where $T = 1/f_0$ is the period determined by the fundamental frequency. The reference has to correspond with the scale and dimension of the actual signal p_{m}. In the mathematical model, the microphone output is some approximation of the pressure fluctulation, whereas in the real experiment, the signal is represented by amplified voltage output from the microphone sensor. Such scaling, as long as it is uniform for both the measured signal and the reference, the only difference to the control design is a constant scaling of the error signal $e_{|P|}$.

Note that in the the design I do not account for the nonlinear microphone transfer function, which is not even considered in the model. Proper identification may improve the performance slightly and alow for isolating the nonlinearities introduced by the sensor from the dynamics of the tube, which, in my setup, are indistinguishable.

The current output from the controller uses a Pulse-Width Modulation (PWM) output for current switching of a DC power supply. I neglect both current dynamics in the power circuit and the load characteristics of the used DC power source. Due to the PWM control and single current direction, the controller output is effectively saturated on $\langle 0, 1\rangle$ and the input to the system is hence $i \in \langle 0, i_\mathrm{h}\rangle$, where $i_\mathrm{h} \approx 3\,\mathrm{A}$ is the switched current, determined by the voltage source and heater resistance via Ohm's law.

For the controller, I tested the variations of a Proportional, Integral and Derivative (PID) regulator on both the real plant and the model. There are two aspects introducing a lag or delay-type character to the feedback, one being the Root Mean Square (RMS) computation in Eq. (5.1) and the other coming from the intergal dynamics of the buoyancy flow. Therefore, derivative D component is used to enable the controller response to the slopes of the error signal $e_{|P|}$ rather than just its value. Figure 5.2 shows the model response to the piecewise linear amplitude reference for PD and PID control. I achieved very similar result with the same couple of controllers on the rijke tube, as shown in Figure 5.3. Except of the slight erratic oscillation in the amplitude, the performance of both controllers is nearly identical. Clearly, the integral component reduces the regulation error and provides better tracking of the linear reference.

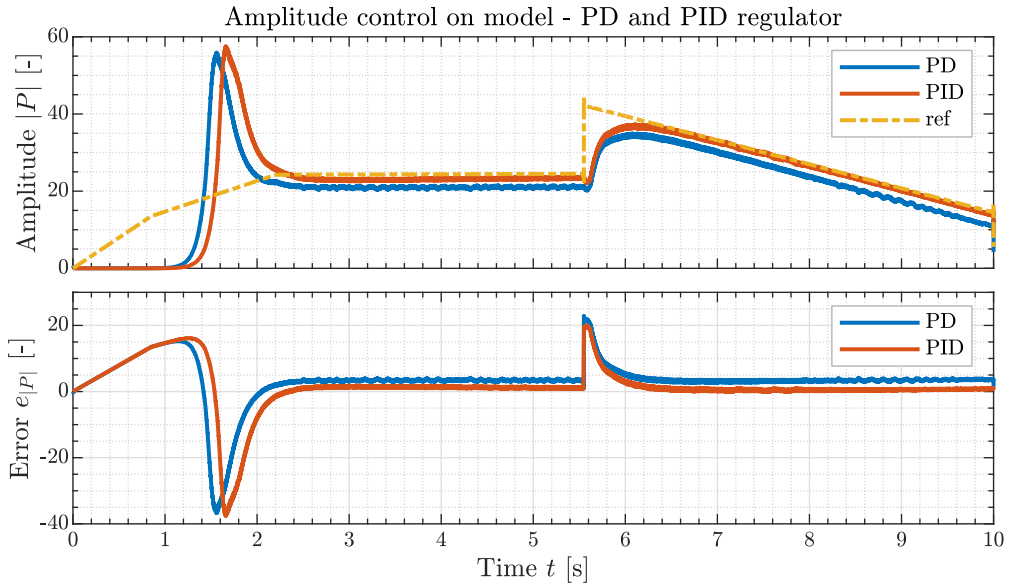

Figure 5.2: Comparison of PD and PID controller performance in amplitude control on the model - piecewise linear reference.

Next, I experimented with control of shorter periodic amplitude pulses, intending to demonstrate the limits of the control solely based on heater current refulation. Model response to a sequence of 2 s wide pulses with is Figure 5.4, promissing relatively good performance in tracking the reference. The response of the physical tube in Figure 5.5 shows, however, that in reality the performance is notably worse, mainly for the PD controller.

Where in model both controllers yielded comparably quick response to the rising edge of the pulses and the only significant difference was in the 'steady' state error, with the real tube there is a massive difference in the transients. First glance it may appear, that the PI controller is somehow more responsive than PD on the rising edges, while the response on falling edge corresponds better with the expected

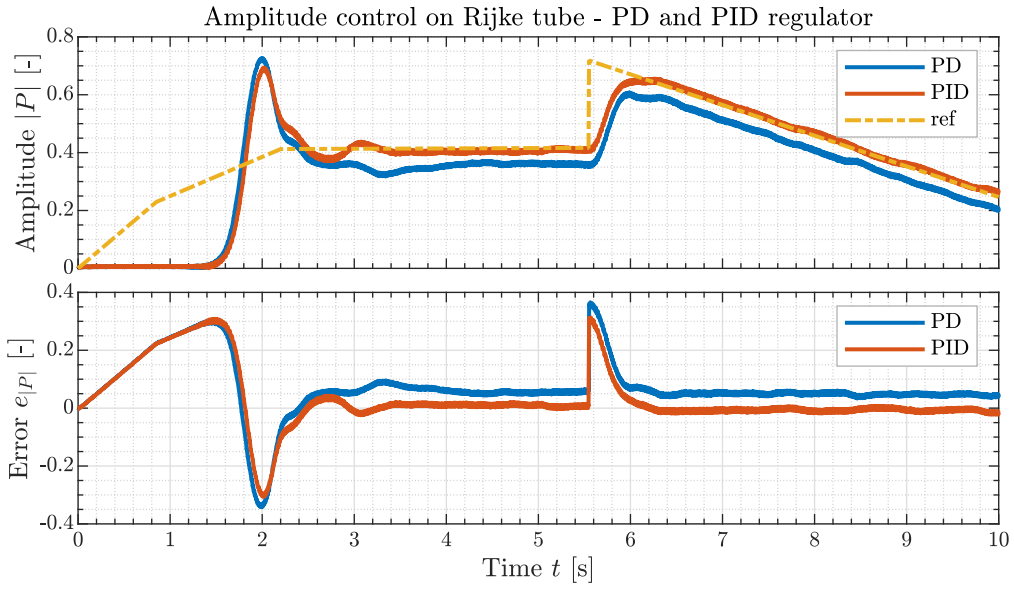

Figure 5.3: Comparison of PD and PID controller performance in amplitude control on the real tube - piecewise linear reference.

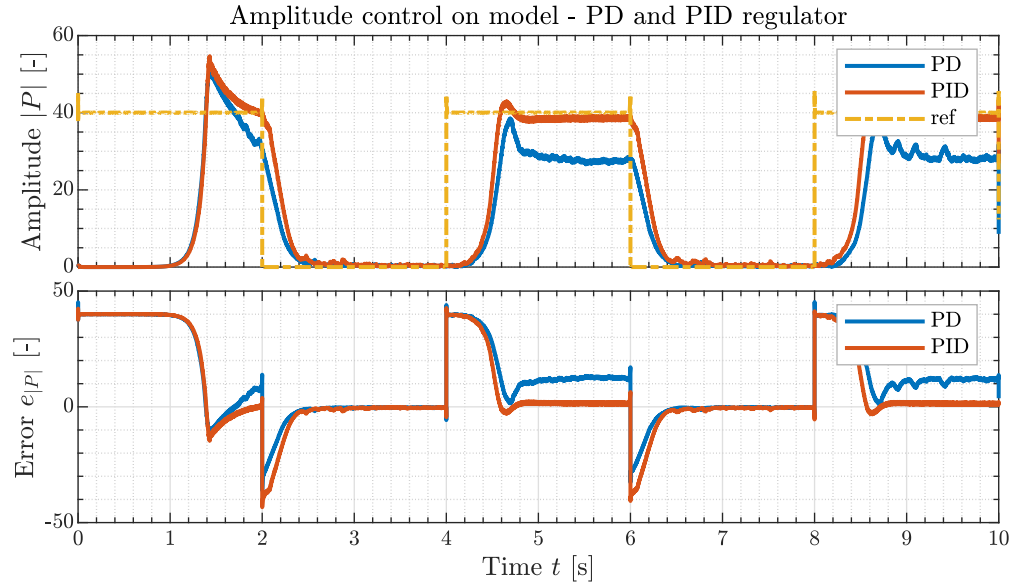

Figure 5.4: Comparison of PD and PID controller performance in amplitude control on the model - 2 s pulse reference.

'lagging' behavior of the additional intergal action. The hint for the explanation of this counter intuitive discrepancy is the inconsistenty of the response of the PID controlled system between the first and consecutive two pulses. While at the first pulse, both controllers perform similarly and the expected lag of PID control is present, the next two pulses feature seemingly faster and better response for PID, whereas PD controller responds relatively consistently. The reason for this becomes apparent upon closer inspection of the amplitude transients between the pulses.

Figure 5.6 shows clearly that the lagging falling edge transient caused by the integral component in PID causes the amplitude to not fully attenuate in between the

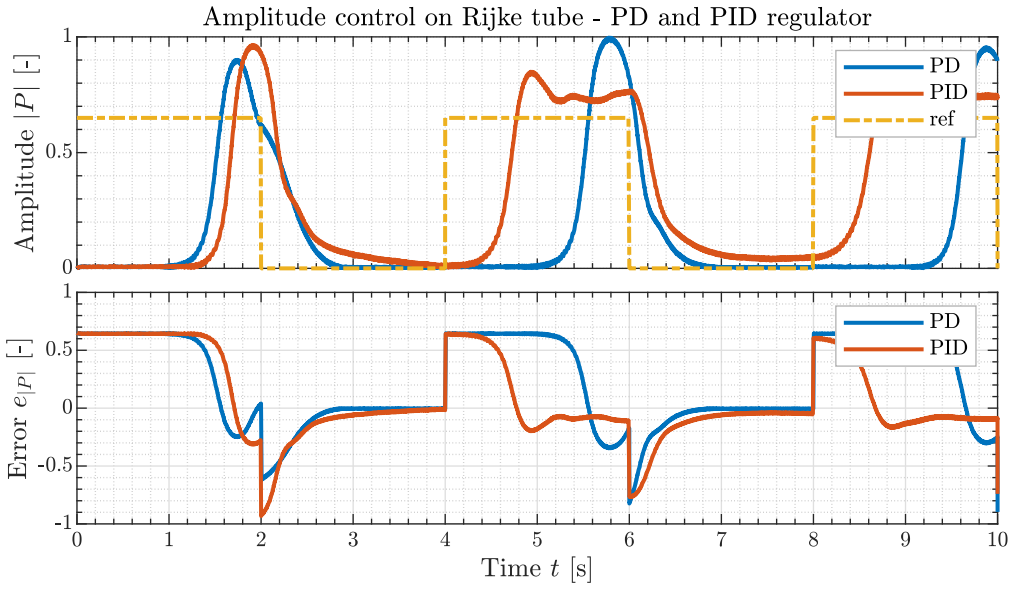

Figure 5.5: Comparison of PD and PID controller performance in amplitude control on the real tube - 2 s pulse reference.

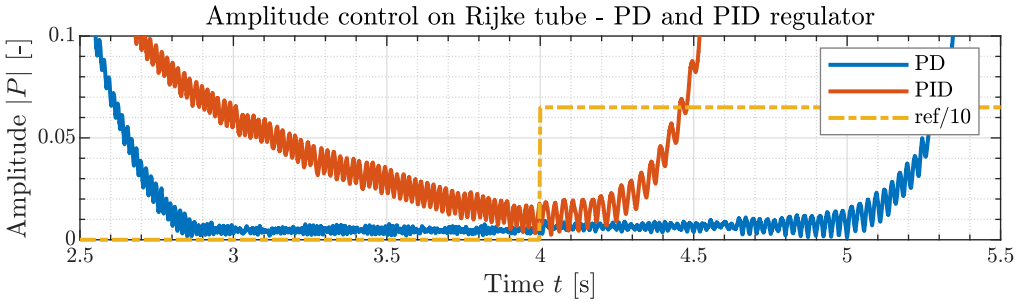

Figure 5.6: Comparison of PD and PID controller performance in amplitude control on the real tube - close view on the transients between pulses.

pulses, and, consequently, sets different initial condition with stronger oscillations at the beginning of the next pulse. As such the attack of the tone is accelerated for the PID controlled system, causing the impression of faster response. The absence of this feature in the model suggests that the accuracy of the modeled response is strongly affected by the initial conditions. Clearly, the attenuation of the oscillations for the simulation with PD controller is insufficient to create the matching initial conditions to the first pulse.

This fact brings several interesting conclusions regarding control w.r.t. musical performance. First, optimal control strategy may differ widely based on the profile of the required amplitude reference signal. For slower transients and longer notes a controller with better tracking error is beneficial, while for faster shorter tones, where in reality the actual intensity of the sound is secondary requirement to the pure presence and absence of it, agile strategy without lagging integral action is better. Moreover, it becomes apparent that regardless the controller choice, heater current control has limited potential in achieving good tracking of faster amplitude pulses, particularly because of the increased requirement for faster decay of the tone into the silence. This is where the acoustic feedback shall improve upon, and eventually offer broader options for heater control strategies.

5.2.1 Idle Heating

Additional feature I implemented to the heater control scheme is the idle heating mechanism. As seen from Figure 5.2 and Figure 5.3, the attack of the tone from no oscillations is slow due to the slow heater and buoyancy flow transients. Therefore, for faster tone triggering, it would be beneficial to maintain some flow and heating even when the tone is not triggered, which should be available with functional acoustic feedback stabilization. The difference in the pulse response of the model with different values of idle heater current is demonstrated in Figure 5.7.

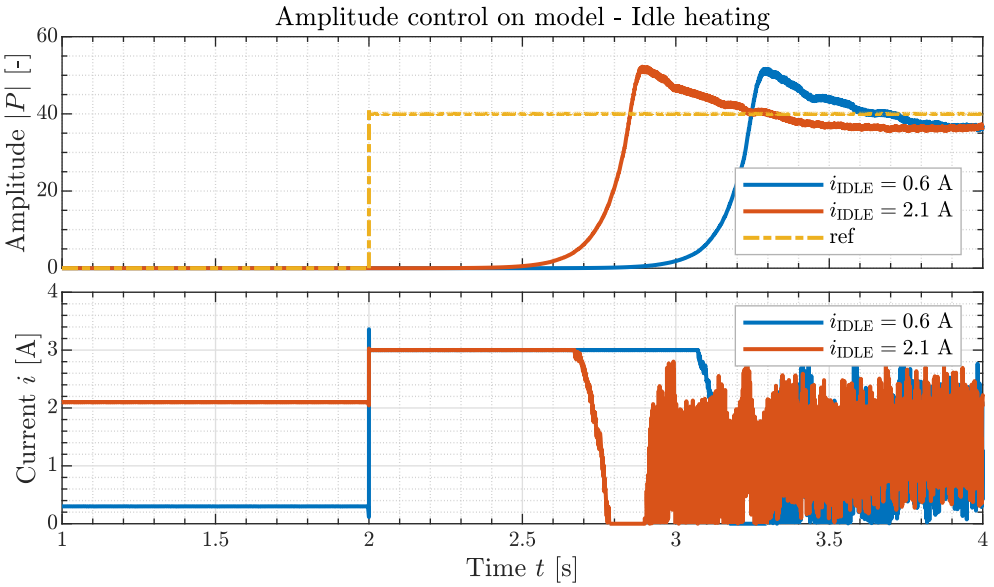

Figure 5.7: Comparison of model responses to amplitude reference pulse for different values of idle heater current.

Implemented switching mechanism gives an option to trigger a value i_{IDLE} of heater current whenever the tone is successfully suppressed, relying upon the abilities of the loudspeaker controller to maintain the established stability even with the increased heat release gain. Optimizing the strategy of when and with what transient should the heater be switched on after the active stabilization takes place is a task warranting its own research. The specification of the ideal performance varies with the intended use of the instrument. For playback performance, this task is a good candidate for optimal and predictive control strategies. For live performance, a control system could be implemented that would allow manual switching between multiple modes of performance, allowing either sharp shot tones or longer decay, similar to the piano pedals.

5.3 Acoustic Control

5.3.1 Feedback

Acoustic feedback control was previously successfully used for stabilizing the acoustic oscillations in the Rijke tube [8, 6, 3, 10]. It turns out that even very simple control architecture consisting of a delayed proportional feedback can be very efficient, which was first demonstrated by Heckl in [8]. This method requires to target a particular mode of the system - typically the fundamental harmonic frequency.

Slightly more advanced controller employing a Time-Delayed Integral (TDI) control logic is presented in [6], which attempts to combat the instabilities over the whole frequency range. The additional integral action, however, brings possible windup issues and is detrimental to the agility of the controller, concerning the speed of attenuation of the oscillations. Other more involved controller designs have been investigated, yet the presented improvement in the performance does not seem to warrant further complexity.

After experimenting with TDI and finding its limits I decided to implement the first mentioned controller along with a simple switching strategy which triggers the controller input and output whenever the reference amplitude is zero. The time shifted (or phase shifted) proportional controller

$$K(s) = -K_P e^{-\tau_K s}\,, \tag{5.2}$$

has two degrees of freedom in its proportional gain K_P and delay τ_K, where $\tau_K \in (0\,,\,1/f_0)$ is the reasonable tuning range for the delay between zero and the period of the oscillation. The stabilizing value is influenced by the geometry of the tube and in the real system also by the distance of the loudspeaker from the tube and the inherent delay of the control circuit. Due to the range of considered controller delays being binded by the signal period, I express the delay as a relative term

$$\tau_C = \tau_K f_0\,. \tag{5.3}$$

I determined the value of the feedback gain empirically based on consecutive experiments. In general, For given τ_C there is a lower boundary the value of K_P for which the controller is stabilizing the system, and typically also an upper boundary, where the feedback destabilizes higher frequency modes in the system. This has been described thoroughly in [6] using CTCR predicted stability maps for the controller.

An important fact to consider when designing the controller gain is the limited output power of the loudspeaker. Moreover, it is not beneficial for the loudspeaker to exhibit highly audible output and corrupt the musical performance of the tube. Therefore, I maintained the values of K_P low enough so the amplitude of the loudspeaker output remains orders of magnitude lower than the tube tone amplitude. Figure 5.8 illustrates the influence of the feedback delay τ_C on the periodically switched sound suppression tested on the mathematical model.

Clearly, the best value is the middle one from the selected range. That suggests similar interval-limited stable values of τ_C, which has been already shown [8], and theoretically backed in [6]. Simplicity of the controller offers the possibilities for future work in automated iterative parameter optimization, which might be applied on the real instrument.

5.3.2 Feedforward

Second utilization of the acoustic control input in the system that I experimented with is the feedforward excitation of the instability. I showed in Section 5.2 that the rise of the oscillation tends to be very slow when only excited by the heat input, in particular if the initial condition features almost no oscillation. I was able to reduce this issue significantly by introducing the idle heating, and appropriately shaped feedforward impulse used to alter the initial condition allows another in this regard.

Similarly to the feedback, my self imposed requirement on low (ideally inaudible) loudspeaker output applies here and directs the selection of the impulse shape on low amplitude impulse with fast decay.

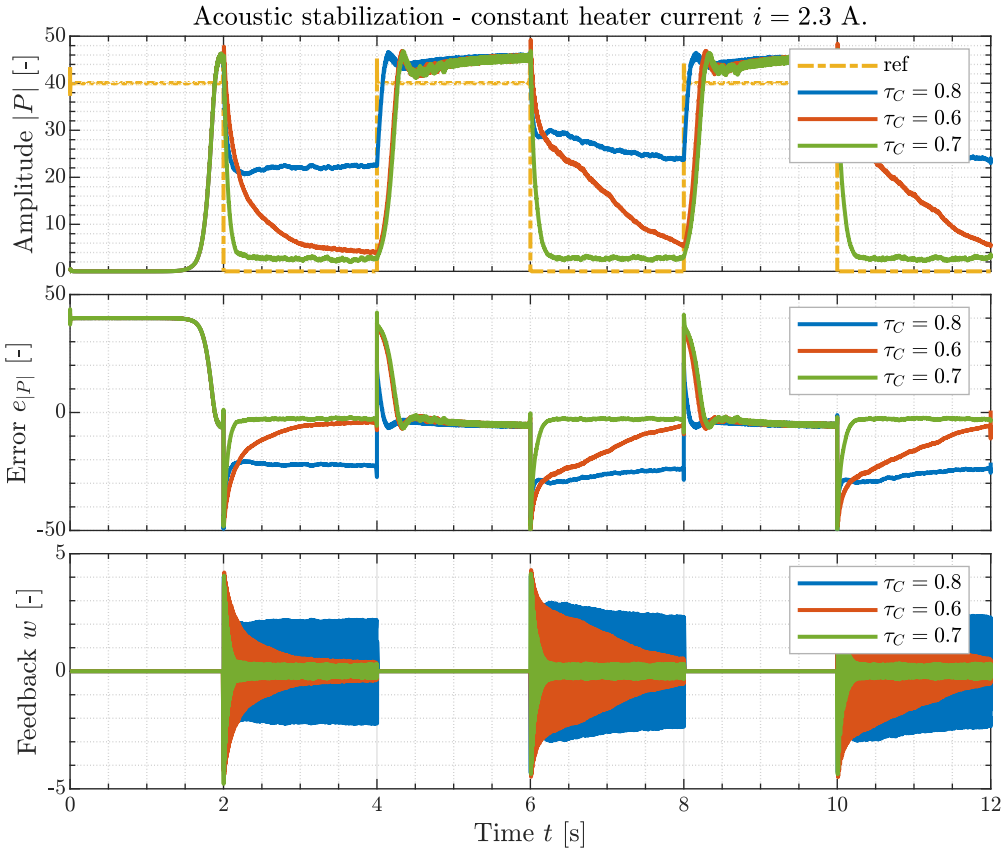

Figure 5.8: Comparison of the performance of the acoustic stabilization on the mathematical model for different values of feedback delay τ_C.

.

I created the feedforward input as a triggered system, excited by a sine wave with the frequency f_0 with the amplitude shaped by a transfer function

$$H_{\text{trig}}(s) = \frac{s}{s+10}\ , \tag{5.4}$$

which provides fast attenuation of the pulse. The performance of the fully featured control system is demonstrated on the model in Figure 5.9. The system can track amplitude pulses with faster period of 2 s thanks to the accelerated attack using feed forward acoustic input. The experiment also shows the importance of the sufficient idle current which enables even faster response to the amplitude pulses.

Last, in Figure 5.10 I show the same experiment executed on the physical Rijke tube. The control scheme is identical, except for the scaling, and the performance is indeed much better than in the experiments with just the heater control.

Interestingly, the subjective perception of the sound of the playing tube does not fully correspond with the plotted magnitude, because of the echo in the room, which is not detected by the microphone, and also because of the approximately logarithmic scale of the human ear sound perception. Hence, the attenuated sound in the off-phases of the amplitude pulses feels louder in reality, than what the visual representation in the plot suggests. It could be interesting to try to incorporate this aspect into the control system by somehow incorporating this logarithmic dependency into the magnitude of the control error.

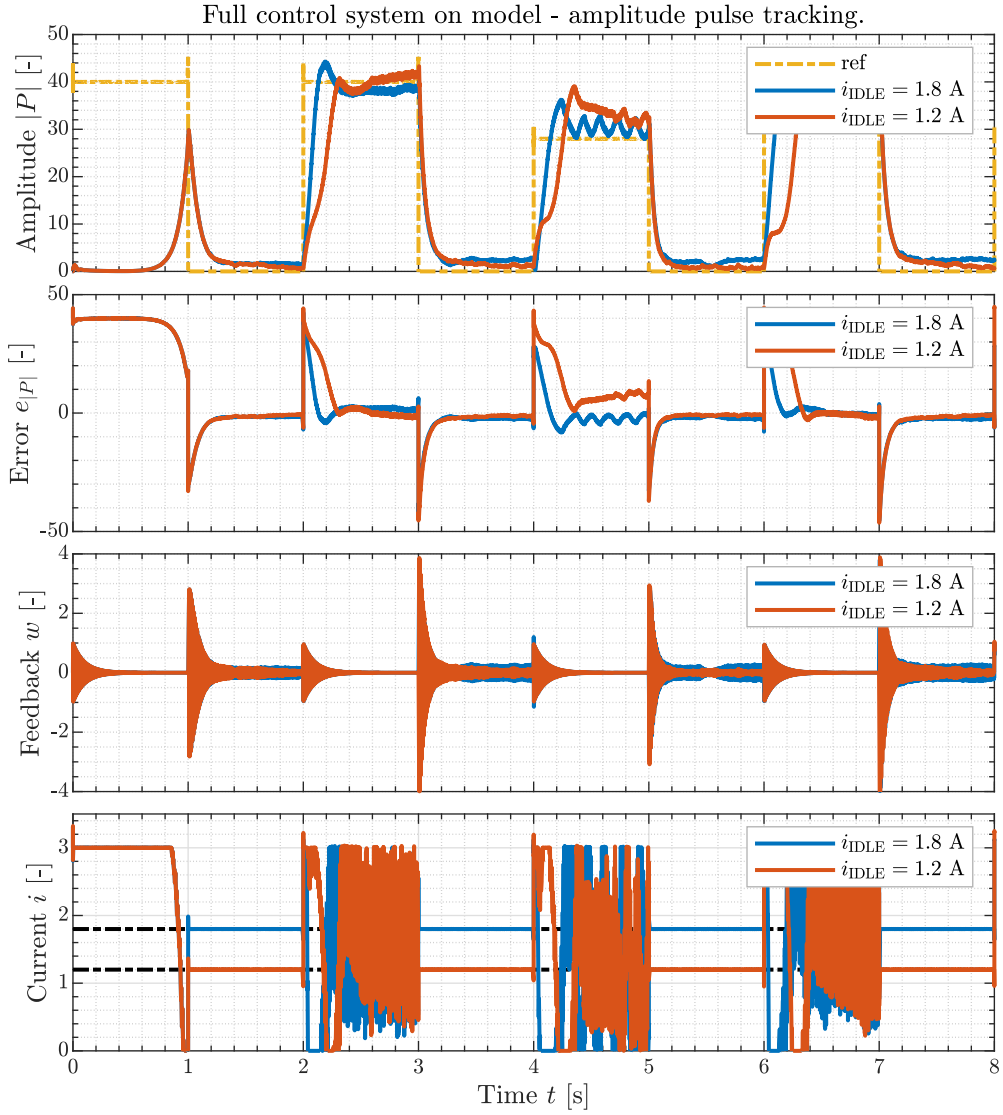

Figure 5.9: Amplitude tracking on mathematical model using the full featured control system.

.

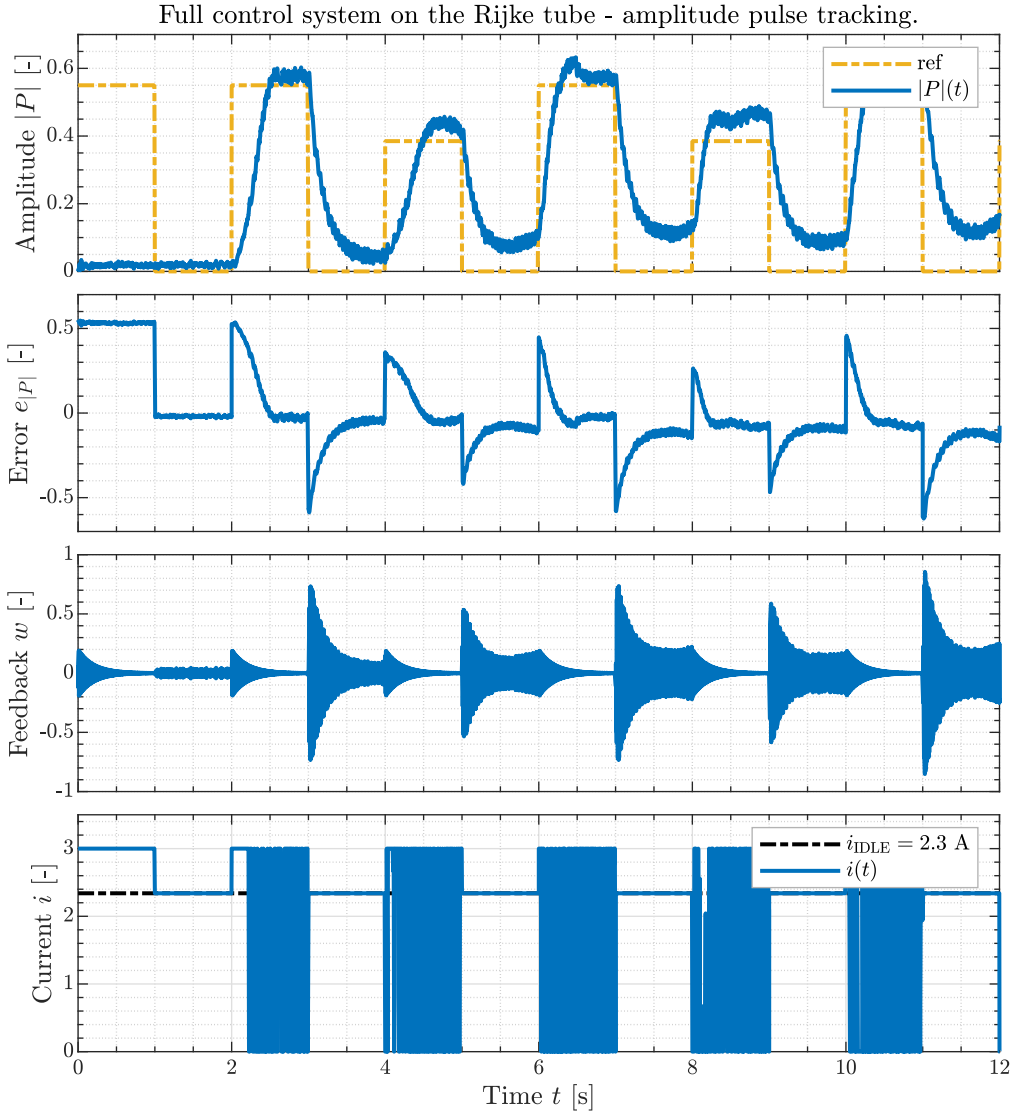

Figure 5.10: Amplitude tracking on the Rijke tube using the full featured control system.

.

6 | Rijke Tube Organ

At the beginning of the design process, I was naturally influenced by the design of the three other Rijke organ builds mentioned in Section **??**, as well as with the typical look of the pipe organ, all of which adopt the in-row topology of the pipes. My initial idea was, therefore, no different and assumed an array of Rijke tubes suspended in a simple stand, each having its own microphone and loudspeaker. Rendering of a 3D drawing sketch in Figure 6.1 portrays this general concept, which takes primary inspiration in the simple organ construction in [23].

Figure 6.1: Original in-line design concept of Rijke tube organ.

Main issue with such design is the requirement for dedicated loudspeaker and its driver for each tube, which would significantly inflate the cost, or, alternatively, limit the selection to cheaper and lower performance components. Therefore I experimented with the idea of single higher performance speaker for controlling multiple tubes, which eventually inspired a completely different design.

6.1 Single Actuator Multi-modal Control

LTI system theory yields an interesting result about systems with single actuator and multiple modes [24, 25]. It turns out that such underactuated system is in fact controllable if all of its modes have different natural frequencies. Moreover,

for just the condition of stabilizability, it suffices that all of the unstable modes have different natural frequencies. Simple example of the application of such result is a linearized model of a 2D system with several inverted pendulums of different moments of inertia mounted on a cart, that can move in horizontal direction.

Good insight this property can be obtained via inspecting Popov-Belevitch-Hautus (PBH) controllability lemma, which is an alternative to the notoriously used rank test of controllability matrix. For general n-th order LTI system described by continuous state-space representation

$$\dot{\mathbf{x}}(t) = \mathbf{A}\mathbf{x}(t) + \mathbf{B}\mathbf{u}(t)\,, \tag{6.1}$$

with vector of states $\mathbf{x}(t)$ and vector of inputs $\mathbf{u}(t)$, the pair $(\mathbf{A}, \mathbf{B})$ is controllable if and only if

$$\operatorname{rank} \mathcal{C}(s) = \operatorname{rank} \left[s\mathbf{I} - \mathbf{A}\,,\, \mathbf{B}\right] = n\,, \quad \forall s \in \mathbb{C}\,. \tag{6.2}$$

Assuming decoupled dynamics, hence diagonal matrix $\mathbf{A}$, for $s = \lambda_i$, where $\lambda_i \in \lambda(\mathbf{A})$ is an eigenvalue of $\mathbf{A}$, the rank of $[s\mathbf{I} - \mathbf{A}]$ clearly reduces by the multiplicity m_i of the eigenvalue λ_i due to null rows. Therefore, in order to maintain the full rank of $\mathcal{C}(s)$, $\mathbf{B}$ has contain corresponding m_i linearly independent rows. For a single input system, however, matrix $\mathbf{B}$ reduces to a row vector, which only has a single linearly independent row. Therefore the maximum multiplicity of any eigenvalue $\lambda(\mathbf{A})$ is $m_\lambda = 1$ in order for the system to be controllable with single input.

Application of such result on the nonlinear system consisting of multiple Rijke tubes is not without risks. The result from LTI theory can be easily spoiled by the existence of actuation limits, which are certainly present here, given the maximum power of the loudspeaker, as well as the nonlinear effects from the tube dynamics. On the other hand, ignoring the nonlinearity of the limit cycle in the tube, the condition of different natural frequencies for the system modes is sufficed for different lengths of the tube. The task of active suppression of the sound in the tube, is in fact a parallel to stabilization in unstable equilibrium.

Another reason that lead me to experiment with this setup is the fact that it is nearly impossible to isolate the effect of tube-specific loudspeaker to just a single tube, unless some acoustic isolation is used in between the tubes. For the setup in Figure 6.1, it would be necessary to consider the influence of at least the two neighboring loudspeakers on each tube and the possible interference of the exerted acoustic pressure waves.

Major downside of the single actuator design, besides the obvious power limit, is the directivity of the loudspeaker, which describes how a speaker's frequency response changes at off axis angles. This is often illustrated through polar magnitude response plots, which show the gain of the speaker for angles from 0° to 90°, where 0° marks the positions on the speaker axis. Typically for increasing frequency and/or circumference of the speaker, the response tends to be more directional and the shape of the response features prominent lobs, denoting that at some particular angles the magnitude of the sound output is close to zero (so called cancellation effect). Example polar plots showing the phenomena are in Figure 6.2.

Placing multiple tubes above single speaker inevitably leads to the off axis position and hence possible issues with cancellation effect and lower efficiency of the loudspeaker induced sound pressure input to the tubes. Moreover, the angle of attack of the pressure waves is askew w.r.t. the axis of the tube, giving an option to some reflections and boundary effects to occur. From my experiments, however, these effects do not seem to strongly influence the overall performance.

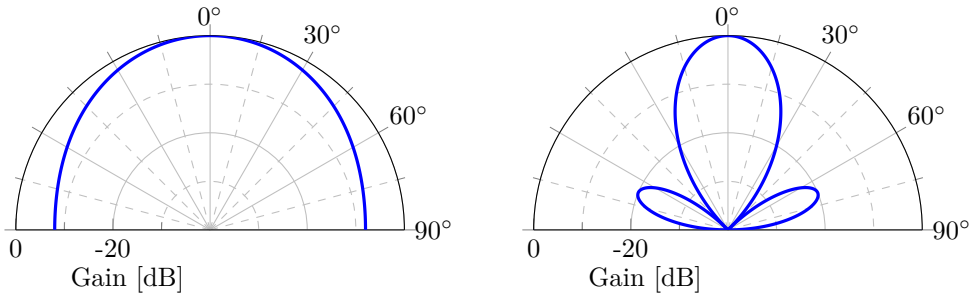

(a) (b)

Figure 6.2: Example polar plots of loudspeaker directivity at lower (a) and higher (b) frequencies.

Within the time scope of this work I was only able to conduct simple tests, measuring the gain of the larger loudspeaker to rule out some extremely undesirable directivity issues. There is certainly a room for improvement in this regard and it is important to be aware of the potential issues detrimental to the control performance. I discuss several possible improvements in terms of the loudspeaker hardware and better sound management in Section 7.2.

Knowing the caveats, I still evaluated the single actuator approach as beneficial from the overall standpoint, taking into account not only the performance aspect but also construction feasibility, cost, and visual appearance. Moreover, such structure potentially offers some additional challenges and interesting problems concerning the control system design. To minimize the negative aspects of this design, I chose tube placement above the heater in a circle with the center coinciding with the speaker axis. As such, the performance should be comparable among the tubes. The vertical distance between the speaker and the bottom end of the tubes was selected such that the off-axis angle is less than 60°.

6.2 Tube Selection

Typical pipe organ setup consist of pipes with such lengths and consequent tones that the range of chromatic scales in several octaves is covered. One chromatic scale consists of 12 tones and for reasonable musical performance, at least several octaves are needed to bring both higher and lower positions to disposal. Given the limited time resources, I decided that attempting to build any more than 12 tubes was not feasible and, I opted for a larger range covering some limited mixture of harmonic scales instead. Another constraint I arbitrarily imposed was regarding the maximum and minimum size of the tube. In order to keep the organ reasonably scaled, I wanted to avoid tubes longer than 1 m, while on the opposite side of the size range, I limited the minimum internal diameter to 33 mm in order to be able to fit the heater and the microphone into the tube.

I consulted the topic of tone selection with Adam Sporka, a musical researcher and professional composer, who has an experience and interest in novel and unorthodox engineering-based musical production. Adam proposed the tube selection according to my specified limits with following commentary:

> “I believe we should start exploring the fitness of its sound in music in bass as well as treble positions. Therefore, the selection of the tones I

have suggested is a compromise between the pitch range and the construction feasibility. The selected pitches will enable to perform a limited set of major and minor chords as well as melodic material. The instrument will be therefore usable for original music where this constraint will be taken into account. This is not unheard of in music: For example, timpani (kettledrums) used in the context of symphonic orchestra are tuned to perform typically only two or four tones out of the given scale."

Selected tones and their respective tube lengths and diameters are in Tab. 6.1. The actual diameters in the physical instrument apparatus vary slightly due to the limits to the supply of the the glass tubing that was available to me at the time.

Table 6.1: List of selected tubes

Tone	**Frequency** f_0 [Hz]	**Length** l_0 [cm]	**Diameter** d_0 [mm]
F_3	174.6	98.0	60
G_3	196.0	87.0	60
C_4	261.6	64.2	60
$C_4^\sharp$	277.2	61.5	60
D_4	293.7	57.9	41
F_4	349.2	48.3	41
G_4	392.0	42.8	41
$G_4^\sharp$	415.3	40.2	41
A_4	440.0	38.3	34
$B_4^\flat$	466.2	36.0	34
C_5	523.3	31.9	34

6.3 Improved Heater Design

When creating a platform with multiple copies of one divide, the question of its practicality and ease and repeatability of fabrication comes to place. As mentioned in Section 4.1 the prototype heater offered sufficient performance, yet was prohibitively time consuming to make and did not allow for easy height adjustment and handling. To improve the first drawback, I experimented with cutting the mica plates using a desktop 40 W CO_2 laser cutter. By experimenting, I found that with low frequency of a laser pulse (typically used for cutting softwood plywood) and low speed, it is indeed possible to cut the mica plates reasonably well, including the narrow slots, however, a manual cleanup is necessary because of the residual bits of mineral. This advancement allowed me to further optimize the shape by introducing a slight outward angle to the slots, which helps to reduce the chance of the wire raising up due to the thermal expansion.

To solve the problem with adjustability, I decided to design the heater element as a removable cartridge that connects to the lead rods via magnets embedded in the ends of the aluminum rods. That allowed me to reduce the length of these rods, which made them easier to handle during the assembly. I machined the 5 mm aluminum rods in several steps, including 1) cutting to rough length, 2) facing both ends and turning to precise length on the metal lathe, 3) cutting the slots for mica cross on the vertical mill, 4) drilling the opposite end on the lathe, and 5) pressing the small magnet into the drilled hole.

For the vertical standoffs I used thin threaded rods, and faced ends on the vertical mill to provide smooth and flat surface to avoid losses of conductivity on the magnetic connection. The threaded rods are mounted in the structure via captive nuts and can be adjusted height-wise for each tube. Once adjusted, a 3D printed spacer is used to maintain the alignment of the heater cartridge. 3D rendering and a photographs of the heater are in Figure 6.3.

(a) (b)

Figure 6.3: 3D model rendering (a) and a photograph (b) of the heater cartridge.

Including the lead in rods, the final heater design has a resistance of 12-13 Ω over the approximate operation temperature range 20-700 °C and the length of the wire in the winding is 0.45 m.

I experimented with larger sizes of the heater to fit the larger diameter tubes, but it turned out that larger footprint with more spread out wire is provides significantly inferior results. Using the same wire loop spacing on larger footprint resulted in higher resistance and consequently lower power, given the limited voltage source. Attempts to counter this issue by using thicker Kanthal wire with higher conductivity introduced larger issues with thermal expansion and I did not record any improvement in the performance. Eventually, I chose uniform heater size that fits the entire set of diameters of used tubes.

6.3.1 Heater Power Supply

The heaters are operated via dedicated PWM switching drivers with maximum input voltage 40 V. PWM duty cycle is determined by the heater control system and delivered to the drivers via digital output ports of the DAQ card. To maximize the power of the heaters given the driver specification, I used a controllable DC switching power supply with output voltage set to 39 V via an analog control signal from the DAQ card.

6.4 Microphone Setup

In Section 3.6 I demonstrated the difference in the measured signal for the downstream and upstream placements and discussed the feasibility of the upstream placement. Possible theoretical small shortcomings are easily compensated for by the significantly higher practicality of this placement. Primarily there is the absence of the need to route the signal wires from the top of the tube and deal with an upper microphone fixture. Upstream placement also allows for the microphone membrane not to face against the direction of the mean airflow, which reduces the consequent wind noise.

Final microphone sensor design uses the smallest commonly available electret microphone cartridge with the 6 mm diameter body which is suspended via 3D printed sleeve on top of 5 mm aluminum tube, which serves as a standoff and also routes the microphone wires. The design fits in with the heater element and its small size prevents from choking the airflow or heavily distorting the reflection of the bottom end of the tube. Similarly to the heater, the microphone allows to be adjusted in height, simply by sliding the aluminum tube up and down through its mounting hole in the organ structure base[1]. The photograph of the sensor is in Figure 6.4.

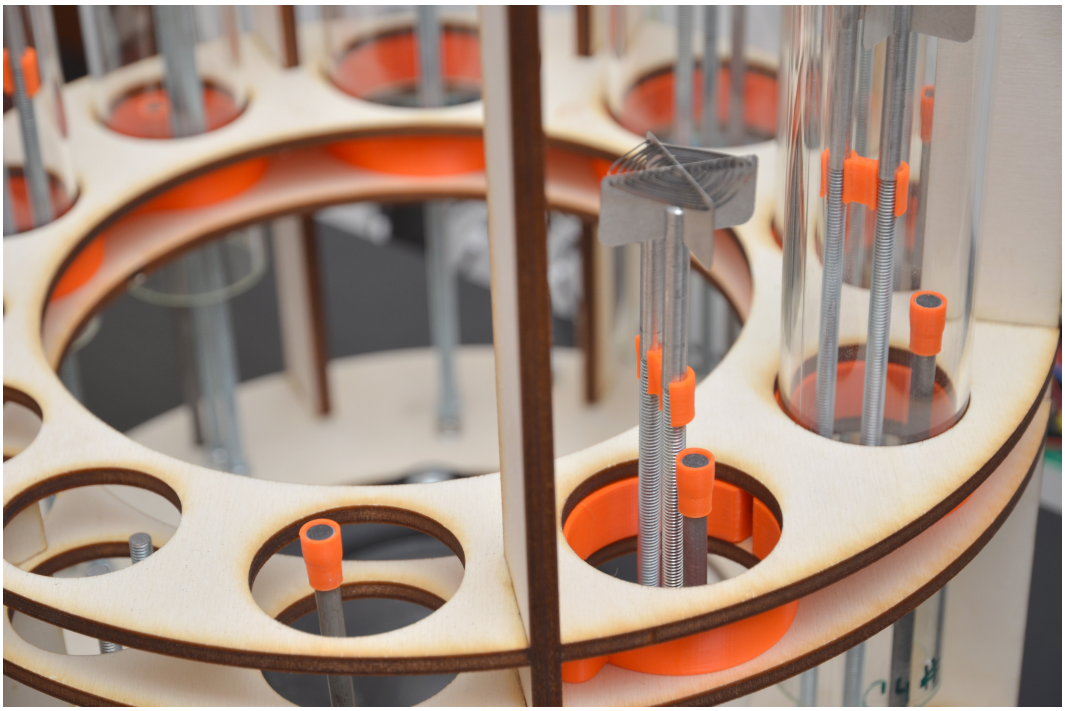

Figure 6.4: Final designed microphone sensors installed in the organ.

To amplify the signal from the small microphones I designed a 11-channel preamplifier board, based on the single channel design used in [21]. The photographs of the completed board are in Figure 6.5.

[1] I faced an unexpected challenge associated with this design choice. The microphones are connected to the preamplifier via standard 3.5 mm audio jack connector, which does not fit through the 5 mm hole. Unwilling to lose the option of quick microphone removal and replacement, I ended up making an intermediary connector made of the 2-pin connectors.

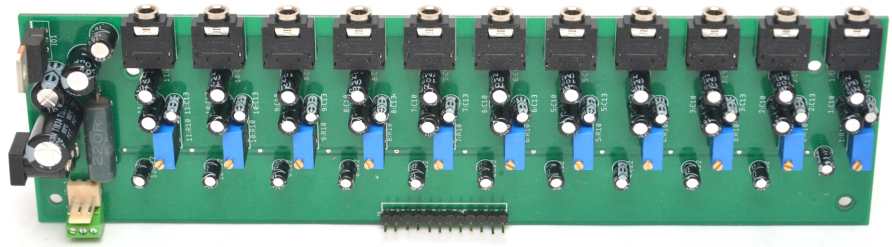

(a)

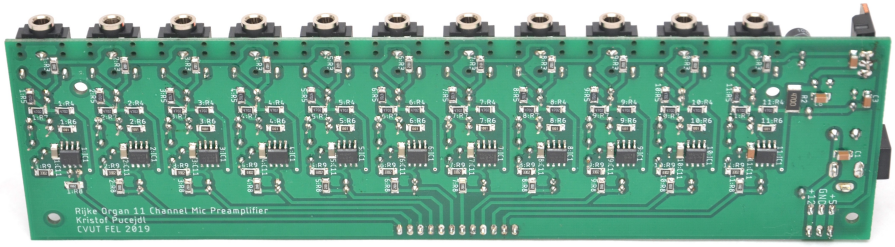

(b)

Figure 6.5: Custom 11-channel microphone preamplifier board: Top side (a) and bottom side (b)

6.5 Organ Structure Design

The overall form of the organ structure needs to follow several requirements imposed by the existing design decisions. It has to securely suspend eleven tubes of different lengths and diameters in a circular arrangement, with a provision for mounting the loudspeaker in the middle of the circle and fixing the rods for heater and microphone components underneath each tube. From mostly aesthetic perspective, I wanted the structure to be reasonably simple and unobstructive, providing a good view of the tubes and the heaters, so the fundamental principle of Rijke tube functioning is not disguised. I also thought about the ease of removal of the tubes for the purposes of servicing the heaters and transport.

In Chapter 4 I mention the 3D printed clamping rings which I designed to hold the tube. These turned out to work so well that I decided to keep the overall concept and embed them into a lightweight cylindrical plywood structure as shown in the Computer Aided Design (CAD) rendered image and a photograph in Figure **??**.

The structure is bolted down to the top of the fabricated stand. The loudspeaker is seated in the opening in the middle of the base ring and it is mounted using customized carriage bolts and custom made foam washers which reduce the mechanical transfer of vibrations from the speaker to the structure. Figure 6.7 shows a 3D printed structure holding the PWM drivers for each heater, which is mounted on the underside of the structure base, and follows the circular arrangement for simpler wire routing. Power source and the rest of the electronics including the fabricated preamplifier are also mounted from underneath the base.

The CAD model rendering of the completed setup is in Figure 6.8 and its real life counterpart in close to finishing state is in Figure 6.9.

(a) (b)

Figure 6.6: 3D model rendering of the upper supporting structure with the tube clamps (a) and a photograph of the real construction (b).

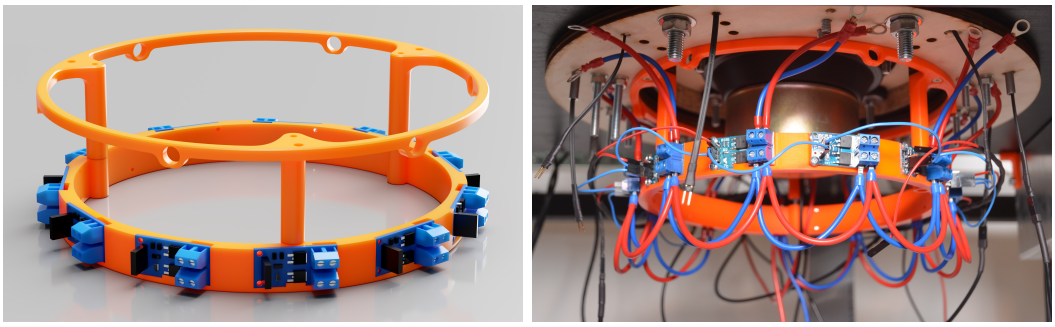

Figure 6.7: 3D model rendering (a) and a photograph (b) of the PWM driver assembly.

Figure 6.8: 3D model rendering of the designed Rijke organ.

Figure 6.9: Photograph of the Rijke organ build.

6.6 Control Performance on the Full Organ

I tested the control system with the Rijke organ with up to seven operational and simultaneously triggered tubes. Unfortunately, used Data Acquisition (DAQ) board[2] in combination with MATLAB® Simulink® did not allow me to log any more than four one dimensional data outputs simultaneously, that is including displaying the signals in virtual oscilloscopes. My own faulty settings might certainly be to blame, but I suspect there is some buffer limit on the board, due to the fact that this limitation did not occur prior to duplicating the control architecture for more than three inputs and outputs. Being unable to provide some graphical representation of the larger scale experiments, allow me, therefore, to provide at least some written description.

The heater control system works for multiple tubes just as well, simply because there is no mutual interference. Moreover there seem to be only little detrimental effect to the abilities of acoustic control by a single loudspeaker due to the acoustic interference.

There is no problem with maintaining the stabilized conditions in up to eight tubes even with a maximum heat input, and the system is able to deal with external disturbance, such as temporary restriction of flow in several tubes, which causes a heat buildup inside these tubes and consequently a strong tendency to destabilize once the airflow is enabled again.

However, and as expected, the performance of the acoustic stabilization starting at unstable initial condition is indeed limited by the power of the loudspeaker output, which effectively prevents simultaneous active attenuation of larger number of tubes. To give some figures, I was able to simultaneously trigger and attenuate three tubes with the tone amplitude being regulated at approximately one third of the maximum volume. For any larger number of tubes or higher amplitudes, the stabilization is still possible, but requires loud audible speaker action and features slow transient.

Note that this is really describing the high demand benchmark testing of the control system and does not imply that the organ can not be useful as an instrument. The requirement of concurrent stabilization of multiple loudly playing tubes can be avoided in the design of the high level control, or in the composition of the music to be performed. In this sense, rather than being just negative, the existence of such performance limit can be perceived as a use determining feature.

[2] Humusoft MF624 PCI input-output board. www.humusoft.cz/datacq/mf624/

7 | Conclusions

The main goal of this thesis was to develop and fabricate a musical instrument based on the Rijke tube. The scale I chose to work in has proven to be very ambitious, given the four months time period I spent working on this thesis to this date. Nonetheless, I was able to design and build a functional the Rijke organ, which at this moment features eight operational Rijke tubes including the automatic control employing both heat source regulation and acoustic excitation and stabilization. I tried to design the organ with higher standards than what would be sufficient for a proof of concept type of device, aiming at better presentability of the final product. Still, there was an inevitable research and development stage, consisting of trial and error and multiple iterations prior to finding plausible solutions. Even though this seeking for quality rendered several of the sub goals stated in the assignment not finished, I am confident that it brought a superior result. Within the development, I successfully derived a mathematical model upon which I was able to test the control system approaches.

The most apparent shortcoming concerning the thesis assignment is the missing implementation of the manual controls of the instrument and the MIDI sequencer interface. The fact that both of these functionalities only make sense if the instrument is otherwise finished and operational has set the priorities for me and I was not able to tackle these sub-tasks in time. Compared to the other aspects of the work, these interface type features are relatively straight forward to implement and I hope to be able to finish both shortly.

7.1 Achieved Results

In Chapter 3, I developed a mathematical model for time domain simulations of the Rijke tube system. Despite being a secondary task in this work, I value the results achieved in mathematical modeling as much as the efforts that went to build the instrument. This is mainly due to the fact that compared to modal-analysis based Rijke tube modeling and control design, time domain simulations are far less investigated. The model is capable of reproducing some of the nonlinear aspects of the thermoacoustic dynamics, and it has proven useful in the initial tests and verifications of the various controller designs.

Chapter 4 documents my experiments with the prototype Rijke tube platform, which I used to determine the final form and design of the structural components and actuators for the organ. The prototype platform allowed me to discover some performance limits and physical restrictions and also provided a reference to the concurrent development of the mathematical model. Moreover, I believe that the designed platform may serve as a good inspiration for building a simple Rijke tube experiment for education.

Based on the experience gained through prototyping, I designed and started

building the current final form of the Rijke organ, which is described in Chapter 6. I finished the instrument for the most part and made it operational so I could to implement and test some of the control strategies described in Chapter 5 which I previously tested on the model and the prototype platform.

The designed control system presents the novel idea of controlling this thermoacoustic system with the objective limiting to stabilization or excitation, but extending to a much broader perspective of musical performance. Despite using relatively simple feedforward and feedback methods, the control system greatly improves the capabilities of the Rijke tube. It enables better control over the tone articulation in terms of its attack and decay as well as the amplitude. The instrument, of course, features numerous limitations, some of which are inherent to its base principle or the current design (e.g., limited number of tubes), and some could be mitigated using the improved control strategies (e.g., insufficient active attenuation of the tone).

7.2 Future Work

7.2.1 Finishing the Organ

Concerning the nearest future of upcoming weeks, I would like to complete the build of the organ by installing the last three missing tubes and improve several temporary solutions in terms of electronics and power supply. I aim to present the device at the Maker Faire Prague 2019[1], and to perform an actual musical piece, rather than just sequences of tones.

Next, there are several bigger improvements I want to incorporate, starting with improving the tune of some of the tones by adjusting the glass tube lengths. Second, following the notes in Section 6.1, I would like to implement higher quality loudspeaker and driver. Possible candidates at the moment appear to be ceiling speakers designed to have good directivity and broad bandwidth. These improvements should enhance the capabilities of the acoustic control and provide a better platform for testing various control approaches.

7.2.2 Model Improvements

There are several aspects in which the mathematical model could be improved. Proper identification of some of the dynamical components stands out as the most lacking regard of the existing model. More accurate description of buoyancy flow dynamics and acoustic reflections coefficients would also warrant the further effort.

7.2.3 Research Topics

One of the unresolved questions in this thesis concerns the change of the microphone placement in the Rijke tube. I propose in Section 3.6 the possible influence of such placement onto the stability regions of the feedback system. Application of respective methods of analysis systems with multiple time delays would provide better insight and to the effects of such topology, should there be any, and possibly bring some valuable findings to the fields concerning the control of thermoacoustic instabilities.

Subjectively, I am most interested in researching the possibilities of predictive strategies for control sequence optimization, based on the desired musical piece to be played on the organ. I lay out the possible options just briefly in Section 5.2. Related

[1] An event celebrating arts, crafts, engineering and science projects. `prague.makerfaire.com`

to this investigation, I want to research options that would enable to account for the logarithmic scale of human ear sound perception. So far, the control system regulates the amplitude in the linear scale, which brings the sensation of a discrepancy between the quality of tracking suggested by the measurements and perceived by hearing.

Bibliography

[1] J.W.S. Rayleigh. The explanation of certain acoustical phenomena. *Nature*, 18(455):319–321, 1878.

[2] Jonathan Peter Epperlein, Santa Barbara University of California, Electrical, and Computer Engineering. *Topics in Modeling and Control of Spatially Distributed Systems*. 2014.

[3] Jonathan Epperlein, B Bamieh, and K.J. Åström. Thermoacoustics and the rijke tube: Experiments, identification, and modeling. *Control Systems, IEEE*, 35:57–77, 2015.

[4] John William Strutt Baron Rayleigh. *The Theory of Sound*. Macmillan, 1894.

[5] Harold Levine and Julian Schwinger. On the radiation of sound from an unflanged circular pipe. *Physical Review*, 73(4):383–406, 1948.

[6] Zalluhoglu Umut and Olgac Nejat. Predicting the secondary dynamic mode interference phenomenon in thermoacoustic instability control. *Proceedings of the Royal Society A: Mathematical, Physical and Engineering Sciences*, 472(2191):20160182, 2016.

[7] M J. Lighthill. The response of laminar skin friction and heat transfer to fluctuations in the stream velocity. *Proceedings of The Royal Society A: Mathematical, Physical and Engineering Sciences*, 224:1–23, 1954.

[8] Maria A. Heckl. Active control of the noise from a rijke tube. *Journal of Sound and Vibration*, 124(1):117–133, 1988.

[9] Umut Zalluhoglu and Nejat Olgac. Passive suppression of thermoacoustic instability in a rijke tube. *IFAC-PapersOnLine*, 49(10):59–64, 2016.

[10] A. M. Annaswamy, M. Fleifil, J. W. Rumsey, R. Prasanth, J. Hathout, and A. F. Ghoniem. Thermoacoustic instability: model-based optimal control designs and experimental validation. *IEEE Transactions on Control Systems Technology*, 8(6):905–918, 2000.

[11] Dan Zhao. Transient growth of flow disturbances in triggering a rijke tube combustion instability. *Combustion and Flame*, 159(6):2126–2137, 2012.

[12] A. P. Dowling. Nonlinear self-excited oscillations of a ducted flame. *Journal of Fluid Mechanics*, 346:271–290, 1997.

[13] P. J. Langhorne. Reheat buzz: an acoustically coupled combustion instability. part 1. experiment. *Journal of Fluid Mechanics*, 193:417–443, 1988.

[14] C. C. Hantschk and D. Vortmeyer. Numerical simulation of self-excited thermoacoustic instabilities in a rijke tube. *Journal of Sound and Vibration*, 227(3):511–522, 1999.

[15] Tomáš Vyhlídal and Pavel Zítek. Mapping based algorithm for large-scale computation of quasi-polynomial zeros. *Automatic Control, IEEE Transactions on*, 54:171–177, 2009.

[16] Tomáš Vyhlídal, Jean-François Lafay, and Rifat Sipahi, editors. *Delay systems: from theory to numerics and applications*. Number 1 in Advances in delays and dynamics. Springer, New York, 2013.

[17] King Louis Vessot and Barnes Howard Turner. Xii. on the convection of heat from small cylinders in a stream of fluid: Determination of the convection constants of small platinum wires with applications to hot-wire anemometry. *Philosophical Transactions of the Royal Society of London. Series A, Containing Papers of a Mathematical or Physical Character*, 214(509-522):373–432, 1914.

[18] Walid Arfaoui, Mohamed Jomaa Safi, and Pierre-Yves Lagrée. Buoyancy-aided convection flow in a heated straight pipe: comparing different asymptotic models. *Heat and Mass Transfer*, 52(8):1515–1527, 2016.

[19] Marc T. Thompson. Chapter 14 - analog low-pass filters. In Marc T. Thompson, editor, *Intuitive Analog Circuit Design (Second Edition)*, pages 531–583, Boston, 2014. Newnes.

[20] Suat Gumussoy, Bora Eryilmaz, and Pascal Gahinet. Working with time-delay systems in matlab®. *IFAC Proceedings Volumes*, 45(14):108–113, 2012.

[21] Černý Lukáš. *Rijkeho trubice - Experimentální zařízení pro modelování a řízení v termoakustice*. PhD thesis, 2017.

[22] S. EVESQUE and A. P. DOWLING. Lms algorithm for adaptive control of combustion oscillations. *Combustion Science and Technology*, 164(1):65–93, 2001.

[23] xofunkox-scientific experiments. Rijke tube organ,orgel.

[24] Panos J. Antsaklis and Anthony N. Michel. *A Linear Systems Primer*. Birkhäuser Basel, 1st edition, 2007.

[25] Thomas Kailath. *Linear Systems*. Prentice-Hall, 1980.